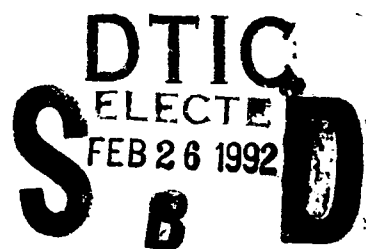


②

# NAVAL POSTGRADUATE SCHOOL

## Monterey, California

AD-A246 464



## THESIS

PHASE TRANSFORMATIONS IN  $Ti_3Al$  BASED ALLOY

by

Emmanuel Tsourdalakis

DECEMBER 1991

Thesis Advisor:

Shantanu Mitra

Approved for public release: Distribution is unlimited

92 2 24 016

92-04676



Unclassified

SECURITY CLASSIFICATION OF THIS PAGE

REPORT DOCUMENTATION PAGE				Form Approved OMB No 0704-0188	
1a. REPORT SECURITY CLASSIFICATION <b>Unclassified</b>			1b. RESTRICTIVE MARKINGS		
2a. SECURITY CLASSIFICATION AUTHORITY			3. DISTRIBUTION/AVAILABILITY OF REPORT <b>Approved for public release: Distribution is unlimited</b>		
2b. DECLASSIFICATION/DOWNGRADING SCHEDULE					
4. PERFORMING ORGANIZATION REPORT NUMBER(S)			5. MONITORING ORGANIZATION REPORT NUMBER(S)		
6a. NAME OF PERFORMING ORGANIZATION <b>Naval Postgraduate School</b>	6b. OFFICE SYMBOL (If applicable) <b>ME</b>		7a. NAME OF MONITORING ORGANIZATION <b>Naval Postgraduate School</b>		
6c. ADDRESS (City, State and ZIP Code) <b>Monterey, CA 93943-5000</b>			7b. ADDRESS (City, State, and ZIP Code) <b>Monterey, CA 93943-5000</b>		
8a. NAME OF FUNDING/SPONSORING ORGANIZATION	8b. OFFICE SYMBOL (If applicable)		9. PROCUREMENT INSTRUMENT IDENTIFICATION NUMBER		
8c. ADDRESS (City, State, and ZIP Code)			10. SOURCE OF FUNDING NUMBER		
			PROGRAM ELEMENT NO.	PROJECT NO.	TASK NO.
11. TITLE (Include Security Classification) <b>PHASE TRANSFORMATIONS IN Ti<sub>3</sub>Al BASED ALLOY</b>					
12. PERSONAL AUTHORS <b>EMMANUEL TSOURDALAKIS</b>					
13a. TYPE OF REPORT <b>Master's Thesis</b>	13b. TIME COVERED FROM _____ TO _____		14. DATE OF REPORT (Year, Month, Day) <b>DECEMBER 1991</b>		15. PAGE COUNT <b>68</b>
16. SUPPLEMENTARY NOTATION <b>The views expressed are those of the author and do not reflect the official policy or position of the Department of Defense or the U.S. Government</b>					
17. COSATI CODES			18. SUBJECT TERMS (Continue on reverse if necessary and identify by block numbers)		
FIELD	GROUP	SUB-GROUP			
19. ABSTRACT (Continue on reverse if necessary and identify by block numbers) <p>A 'super <math>\alpha_2</math>' Ti<sub>3</sub>Al based alloy with additions of niobium, chromium and tantalum was studied with respect to phase transformations under different heat treatments and aging times and temperatures. As received samples were heated at temperatures ranging between 1000 °C and 1300 °C and quenched to retain the high temperature microstructure. Quenched samples were aged between 500 °C and 850 °C for various times and transformations were studied using dilatometry, x-ray analysis, transmission electron microscopy and microhardness testing.</p> <p>It was found that at around 650 °C the transformation of <math>\beta \rightarrow \alpha_2</math> occurred after two hours of aging, while below this temperature, aging for up to 100 hours at 500 °C produced only the <math>\beta \rightarrow \omega</math> transformation with very little <math>\alpha_2</math>. Also, an '<math>\omega</math>-type' phase was observed at this aging temperature. Microhardness measurements and x-ray diffraction confirmed the above results. Quenching from high temperature showed the presence of lath-like features which were poor in Ta and Cr and had the B2 structure. Finally, some regions with an orthorhombic structure were observed in the as quenched samples. Overall, peak hardness was obtained after aging the quenched <math>\beta</math> phase sample at 650 °C. This corresponded to a microstructure of retained <math>\beta</math> with a fine acicular structure of <math>\alpha_2</math>.</p>					
20. DISTRIBUTION/AVAILABILITY OF ABSTRACT <b>XX UNCLASSIFIED/UNLIMITED</b> <input type="checkbox"/> SAME AS RPT <input type="checkbox"/> DTIC USERS			21. ABSTRACT SECURITY CLASSIFICATION <b>unclassified</b>		
22a. NAME OF RESPONSIBLE INDIVIDUAL <b>Shantanu Mitra</b>			22b. TELEPHONE (Include Area Code)		22c. OFFICE SYMBOL <b>ME/Mt</b>

Approved for public release: Distribution is unlimited

Phase Transformations in  $Ti_3Al$  Based Alloy

by

Emmanuel Tsourdalakis  
Lieutenant, Hellenic Navy  
B.S., Hellenic Naval Academy, 1983

Submitted in partial fulfillment of the  
requirements for the degree of


MASTER OF SCIENCE  
IN MECHANICAL ENGINEERING

from the

NAVAL POSTGRADUATE SCHOOL

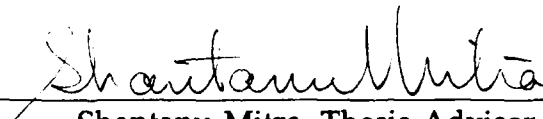
DECEMBER 1991

Author:

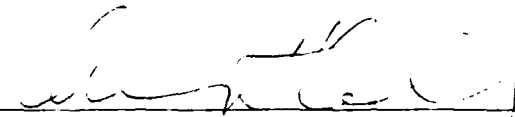


Emmanuel Tsourdalakis

Approved by:



Shantanu Mitra, Thesis Advisor



A.J. Healey, Chairman  
Department of Mechanical Engineering

## ABSTRACT

A 'super  $\alpha_2$ '  $\text{Ti}_3\text{Al}$  based alloy with additions of niobium, chromium and tantalum was studied with respect to phase transformations under different heat treatments and aging times and temperatures. As received samples were heated at temperatures ranging between 1000 °C and 1300 °C and quenched to retain the high temperature microstructure. Quenched samples were aged between 500 °C and 850 °C for various times and transformations were studied using dilatometry, x-ray analysis, transmission electron microscopy and microhardness testing. It was found that at around 650 °C the transformation of  $\beta \rightarrow \alpha_2$  occurred after two hours of aging, while below this temperature, aging for up to 100 hours at 500 °C produced only the  $\beta \rightarrow \omega$  transformation with very little  $\alpha_2$ . Also, an ' $\omega$ -type' phase was observed at this aging temperature. Microhardness measurements and x-ray diffraction confirmed the above results. Quenching from high temperature showed the presence of lath-like features which were poor in Ta and Cr and had the B2 structure. Finally, some regions with an orthorhombic structure were observed in the as quenched samples. Overall, peak hardness was obtained after aging the quenched  $\beta$  phase sample at 650 °C. This corresponded to a microstructure of retained  $\beta$  with a fine acicular structure of  $\alpha_2$ .

iii



Accession For	
NTIS GRA&I	<input checked="" type="checkbox"/>
DTIC TAB	<input type="checkbox"/>
Unannounced	<input type="checkbox"/>
Justification	
By	
Distribution/	
Availability Codes	
Dist	Avail and/or Special
A-1	

## TABLE OF CONTENTS

I.	INTRODUCTION .....	1
II.	BACKGROUND .....	3
	A. PHASE TRANSFORMATIONS IN Ti-Al ALLOYS .....	3
	1. General Remarks .....	3
	a. $\beta \rightarrow \alpha_2$ Transformation .....	3
	b. $\beta_{\text{retained}} \rightarrow \omega$ Transformation .....	7
	2. Effect of Cooling Rates on Phase Transformations .....	9
	B. EFFECT OF ALLOYING ELEMENTS ON PHASE TRANSFORMATIONS AND MECHANICAL PROPERTIES .....	11
	1. Effect on Phase Transformations .....	11
	2. Effect on Mechanical Properties .....	12
	3. Alloy Design .....	15
	C. X-RAY DIFFRACTION .....	16
	D. SCOPE OF PRESENT STUDY .....	17
II.	EXPERIMENTAL PROCEDURE .....	19
	A. HEAT TREATMENTS .....	19
	B. MICROSCOPY .....	20
	1. Optical and Scanning Electron Microscopy .....	20
	2. Transmission Electron Microscopy .....	20
	C. DILATOMETRY .....	21
	D. X-RAY DIFFRACTOMETRY .....	21
	E. MECHANICAL TESTING .....	22
IV.	RESULTS .....	23
	A. MICROHARDNESS TESTING .....	23
	B. X-RAY DIFFRACTION ANALYSIS .....	25

C. MICROSCOPY OF HEAT TREATED SAMPLES .....	29
1. 1200 °C and Quenched .....	29
2. As Quenched and Aged at 500 °C for 9h .....	36
3. As Quenched and Aged at 650 °C for 48h .....	40
4. As Quenched and Aged at 850 °C for 48h .....	42
D. DILATOMETRY .....	46
V. CONCLUDING REMARKS .....	52
LIST OF REFERENCES .....	54
INITIAL DISTRIBUTION LIST .....	57

## LIST OF TABLES

TABLE I.	PROPERTIES OF HIGH TEMPERATURE ALLOYS . . . . .	14
TABLE II.	AS EXTRUDED MECHANICAL PROPERTIES OF Ti-Al ALLOYS . . . . .	16
TABLE III.	PEAK POSITIONS AND RELATIVE INTENSITIES . . . . .	25

## LIST OF FIGURES

Figure 1.	Ti-Al Phase Diagram . . . . .	5
Figure 2.	The Hexagonal Close Packed $DO_{19}$ Structure . . . . .	6
Figure 3.	The Linear Fault Model for $\omega$ Transformation, Showing Equal and Opposite Shear Forces Applied on Adjacent (110) $_{\beta}$ Planes. . . . .	8
Figure 4.	Mottled Microstructure of $\omega$ Phase in $Ti_3Al$ (Top) and Showing Streaking when Imaged in Two Beam Condition with $g=\langle 110 \rangle_{\beta}$ (Bottom) . . . . .	10
Figure 5.	Effect of Cooling Rate in $Ti_3Al-Nb$ from the $\beta$ Region on Microstructure: (a) $\beta$ /Air Cooling, (b) $\beta$ /Controlled Cooling, (c) $\beta$ /Slow Cooling. . . . .	11
Figure 6.	$Ti_3Al+Nb$ ternary section [Ref. 17] . . . . .	13
Figure 7.	Diffraction of X-Rays by a Crystal . . . . .	17
Figure 8.	Vickers Microhardness of Quenched and Aged Samples vs Aging Time . . . . .	24
Figure 9.	SEM Micrographs of the Samples Aged at 750°C (Top) and 850°C (Bottom) Showing Coarsening Effect Between the Two Temperatures . . . . .	26
Figure 10.	Diffractometer Output of Relative Intensities vs Angle 2 $\theta$ for the As Quenched and the Samples Aged at 500°C for 4 and 24 Hours . . . . .	27
Figure 11.	Nelson-Riley Extrapolation for Lattice Parameter 'a' . . . . .	30
Figure 12.	XRD Scans for the Sample Aged at 650°C for 2h (Top) and 24h (Bottom) . . . . .	31
Figure 13.	XRD Scans for the Sample Aged at 750°C for 2h (Top) and 24h (Bottom) . . . . .	32



Figure 14.	Bright Field from the Sample Heated at 1200 °C and Quenched, Showing High Dislocation Density Along with some Lath-Like Features . . . . .	34
Figure 15.	SADP [001] $\beta$ Zone Showing Streaking Along $\langle 110 \rangle \beta$ and Superlattice Reflections at $\langle 100 \rangle$ . . . . .	35
Figure 16.	TEM micrograph from the As Quenched Sample Showing Mottled Contrast in Both the Lath and the Surrounding Matrix. Note Low Angle Grain Boundary Formed by Dislocation Array . . . . .	35
Figure 17.	Selected Area Diffraction Pattern, [113] $\beta$ Zone from the Matrix . . . . .	36
Figure 18.	EDXS from Regions Inside (Top) and Outside (Bottom) a Lath, from the Sample Heated at 1200°C and Quenched . . . . .	37
Figure 19.	Selected Area Diffraction Pattern [001] $\alpha$ Zone . . . . .	38
Figure 20.	SEM Micrographs of the Sample Heated at 1300°C for 4h and Quenched, from Regions at the Center (Top) and Near the Surface (Bottom) . . . . .	39
Figure 21.	Mottled Structure from the Sample Aged at 500°C for 9h . . . . .	40
Figure 22.	Selected Area Diffraction Pattern [111] $\beta$ Zone . . . . .	41
Figure 23.	Selected Area Diffraction Pattern [001] $\beta$ Zone . . . . .	41
Figure 24.	Selected Area Diffraction Pattern [113] $\beta$ Zone . . . . .	42
Figure 25.	Dark Field TEM Micrograph of the Sample Aged at 650 °C Showing a Fine Needle-like Structure Due to the Formation of the $\alpha_2$ Phase . . . . .	43
Figure 26.	Selected Area Diffraction Pattern [113] $\beta$ Zone . . . . .	43
Figure 27.	Bright Field of the Sample Aged at 850°C for 48h Showing a Phase Mixture of $\alpha_2$ Laths and $\beta$ (with the $\omega$ -type phase) . . . . .	44

Figure 28.	Selected Area Diffraction Pattern $[113]\beta$ zone, with $1/3\langle 112 \rangle$ Spot Pointed and Used for CDF in Figure 29 .....	45
Figure 29.	Centered Dark Field of the Sample Aged at $850^{\circ}\text{C}$ for 48h With the $1/3\langle 112 \rangle\beta$ Type Spot Marked in Figure 28 .....	45
Figure 30.	Dilatometry Curves of the As Quenched Sample. Heating (Bottom Curve) at a Rate of $2.5^{\circ}\text{C}/\text{min}$ and Cooling at a Rate of $1.8^{\circ}\text{C}/\text{min}$ . ....	49
Figure 31.	Continuous Cooling Transformation Diagram for the High Temperature $\beta$ Phase .....	50
Figure 32.	Dilatometry Curves of Slow Heating up to the $\beta$ Region and Subsequent Cooling at a Rate of $160^{\circ}\text{C}/\text{min}$ . ....	51

## I. INTRODUCTION

Titanium alloys and more specifically titanium aluminides are very promising materials that have been developed during the last two decades, for the aerospace industry and high temperature applications. The reasons for their attractiveness are i) their high strength at elevated temperatures, ii) their excellent corrosion resistance and iii) their substantially lower density compared with the superalloys and steels. The main drawback for the usage of these alloys is their poor room temperature ductility. Recently, titanium aluminides with Al content ~25 at. % and with ternary and quaternary additions of the so called  $\beta$ -stabilizers, have drawn a lot of attention, in an attempt to overcome this problem.

A major portion of the research in this area is centered on the microstructural changes and the associated mechanical properties through the study of the phase transformations that this type of alloy exhibits. An ideal combination of the high temperature relatively ductile phase ( $\beta$  phase) and the room temperature strong hexagonal close packed phase ( $\alpha_2$  phase) is sought through proper alloy design. This would still give the desired strength at elevated temperatures along with better room temperature ductility. Besides this, alloying additions to further improve oxidation resistance have been envisioned.

The work in this thesis, involves the study of some the phase transformation and the accompanying changes in mechanical properties in a Ti-30 Al-8 Nb-2 Ta-2 Cr alloy, which is based in the  $Ti_3Al$  phase field of the Ti-Al phase diagram.

## II. BACKGROUND

### A. PHASE TRANSFORMATIONS IN Ti-Al ALLOYS

#### 1. General Remarks

Among Ti-based alloys, one of the most attractive in terms of mechanical properties and corrosion resistance, is the Ti-Al system. The increasing interest in this system, in recent years, is due to its exceptional mechanical properties at high temperatures. Low ductility values below 600°C still limit its use in many engineering applications. The main reason for the Ti rich Ti-Al based alloys' low ductility is the ordered hexagonal  $\alpha_2$  phase that exists at room temperature. The improvement of the room temperature properties of the Ti-Al system, without significant losses of its high temperature properties, involves the understanding of the phase transformations in this system. Many different phase diagrams have been proposed for the Ti-Al system since 1951, when Ogden et al. [Ref. 1] completed the Ti-rich side of the diagram. The most recent is the one by Murray [Ref. 2] shown in Figure 1. The three major phase transformations at the Ti-rich end of the diagram are,  $\beta \rightarrow \alpha$  or  $\alpha_2$ ,  $\beta \rightarrow \beta_{\text{retained}} \rightarrow \omega$  and  $\beta_{\text{retained}} \rightarrow \alpha$  or  $\alpha_2$ .

##### a. $\beta \rightarrow \alpha_2$ Transformation

The high temperature bcc phase  $\beta$ , in the Ti rich side of the phase diagram can undergo a number of transformations. This phase can be either

ordered (B2) or disordered and this can affect the transformation products accordingly.

The  $\beta \rightarrow \alpha_2$  transformation, in most Ti alloys centered around the  $\text{Ti}_3\text{Al}$  composition, can be martensitic if the  $\beta$  phase is quenched and no  $\beta$  stabilizing alloying additions are present. Also decomposition of the  $\beta_{\text{retained}}$  phase can occur during aging when  $\beta$  stabilizers allow for retention of  $\beta$  on quenching.

There are four different types of martensite that have been identified [Ref. 3]. The most common is a cubic to hexagonal transformation, characterized by a habit plane near  $\{334\}_\beta$ . This type of martensite is found in pure Ti and dilute Ti alloys. Two other types of martensite, usually found in more concentrated alloys are, a) formed with a habit plane near  $\{344\}_\beta$  and b) formed by degeneration of the hexagonal structure of the product phase to an orthorhombic structure. Finally the fourth type has an fcc or fct structure [Ref. 3].

In the composition range of 30 at.% Al, the room temperature phase is an ordered  $\alpha_2$  based on  $\text{Ti}_3\text{Al}$ . This phase has a  $\text{DO}_{19}$  structure [Ref. 4] as shown in Figure 2.

During quenching from the high temperature  $\beta$ -field, full retention of the  $\beta$  phase is possible in alloyed Ti. This also true for the  $\text{Ti}_3\text{Al}$  based phase. Subsequent aging of the  $\beta_{\text{retained}}$  phase at elevated temperatures causes the formation of the stable  $\alpha$  phase or the ordered  $\alpha_2$  phase.

Banerjee *et. al.* [Ref. 5] have recently identified another phase in the  $\text{Ti}_3\text{-Al-Nb}$  system heat treated at temperatures below  $1253^\circ\text{C}$ , which has an

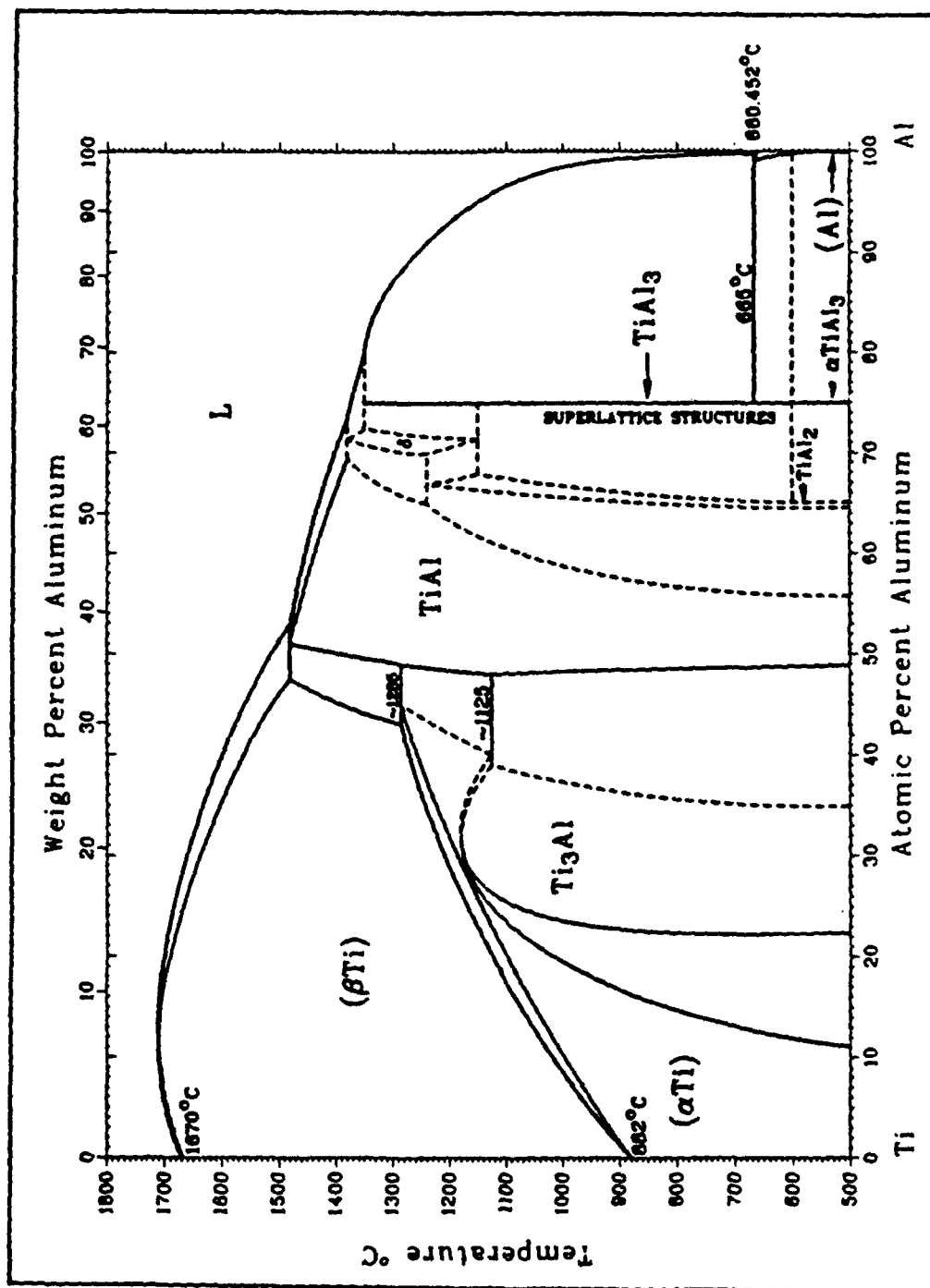
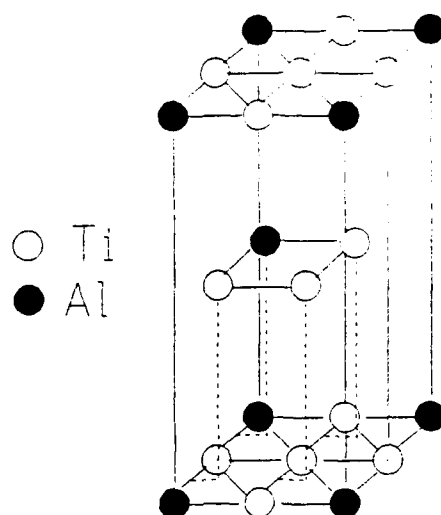


Figure 1. Ti-Al Phase Diagram



**Figure 2. The Hexagonal Close Packed DO<sub>19</sub> Structure**

ordered orthorhombic structure with a Cmc<sub>2</sub>m symmetry, and in which the Nb atoms occupy a sublattice distinct from the Ti and Al atoms. This phase is often called 'O' phase and is derived from a distortion of the 'a' and 'c' axes of the close packed hexagonal  $\alpha_2$  phase. This 'O' phase is also seen at the interface between  $\beta$  and  $\alpha_2$  phases in the plate form, where the Nb atoms do not occupy a distinct sublattice, but substitute for Ti atoms [Ref. 6]. Some evidence of the amphoteric nature of Nb is also available which identifies Nb with both the Ti and Al sublattice. Other researchers [Ref. 7] believe that the O phase occurs at the  $\alpha_2/\beta$ (B2) interface due to hydrogen absorption during thin foil preparation in an acid containing electrolyte, for heat treatments above 1253 ° K.



**b.  $\beta_{\text{retained}} \rightarrow \omega$  Transformation**

The  $\beta_{\text{retained}}$  phase is metastable at room temperature and in many Ti alloys tends to decompose after aging. The decomposition products depend on the aging temperature can be either the  $\alpha$  or  $\omega$ -phase.

The transformation to the  $\omega$  phase, which does not appear on the phase diagram, [Ref. 8] is closely related to the martensitic transformation in terms of soft mode lattice dynamics. According to de Fontaine [Ref. 9] the  $\omega$  phase, requires the high temperature  $\beta$  bcc lattice to be unstable with respect to longitudinal phonons centered about  $2/3\langle 111 \rangle$ . The first observations [Ref. 10] on the occurrence of this phase were made during 1950s and showed  $\omega$  phase to occur athermally during rapid quenching from the high temperature  $\beta$  phase, similar to martensite, by a series of atomic shuffles. Its structure was identified to be either hexagonal or trigonal, depending on solute concentration in Ti alloys. The relationship between  $\omega$  phase and the parent lattice [Ref. 10] defined by:

$$(0001)_{\omega} | (111)_{\beta} ; [2\bar{1}\bar{1}0]_{\omega} | [1\bar{1}0]_{\beta}$$

Two models have been proposed for the  $\omega$  phase transformation. The first is the linear fault model, shown in Figure 3, which states that the transformation occurs by applying an equal and opposite shear force in the  $\langle 111 \rangle_{\beta}$  direction, to pairs of adjacent  $(110)_{\beta}$  planes in the bcc lattice. The second model is the dynamical equivalent of the linear fault model. This states that, in order for the shifting of the adjacent planes to occur (Figure 3), a longitudinal

wave of wavelength equal to the separation of the  $(111)_\beta$  planes is needed, that is a longitudinal phonon with wave vector  $2/3\langle 111 \rangle$ .

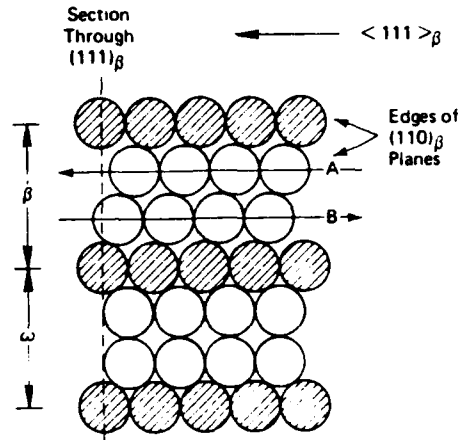


**Figure 3. The Linear Fault Model for  $\omega$  Transformation, Showing Equal and Opposite Shear Forces Applied on Adjacent  $(110)_\beta$  Planes**

The second type of  $\omega$  phase identified, is the diffuse- $\omega$ . The first, athermal  $\omega$ , is caused by the instability of the bcc lattice with temperature, and is affected by concentration, combined with the  $2/3\langle 111 \rangle$  phonon, whereas the second, diffuse  $\omega$  is believed to be caused by the longitudinal  $2/3\langle 111 \rangle$  phonon only [Ref. 11].

During recent years many investigators trying to characterize certain anomalies of the  $\beta$  (ordered, disordered) phase discovered that these anomalies are closely related to the formation of the  $\omega$  phase. Perkins et al. [Ref. 12], using transmission electron microscopy observed, in many quenched and aged beta-brass type alloys, mottling, striations, diffuse streaking and extra

maxima in certain positions of electron diffraction patterns. Figure 4 shows typical contrast effects of the  $\omega$ -type phase in the Ti-Al alloys [Ref. 13]. The  $\omega$  phase can be thought of as a transformed  $\beta$  phase (inheriting its order or disorder) and a precursor to the  $\alpha$  phase which forms on further heating (aging).

Strychor *et. al.*, [Ref. 13] have shown that the ordering of the  $\beta$  phase can impart extra spots to the electron diffraction pattern of the  $\omega$  phase in the  $\text{Ti}_3\text{Al-Nb}$  alloy. Spots at  $1/3\langle 112 \rangle$  in the  $[110]\beta$  zone axis can only be explained by the ordered hexagonal structure of  $\omega$ , called  $\omega'$ . Furthermore the aging experiments of Strychor *et. al.*, [Ref. 13] were only carried out up to 500 °C with no information existing on the temperature and kinetics of other transformations at higher aging temperatures. Hence one of the objectives of this study was to investigate the transformation kinetics and the reaction products of the retained  $\beta$  phase at temperatures greater than 500 °C in an alloyed quaternary 'super  $\alpha_2$ ' titanium aluminide.

## **2. Effect of Cooling Rates on Phase Transformations**

Studies on Ti-Al systems [Ref. 14] revealed a dependence of the phase transformation temperatures on the cooling rates. Quenching from the  $\beta$ -field at low cooling rates (around 10 °C/s), resulted in the acicular  $\alpha_2$  with no evidence of retained  $\beta$  phase. Conversely at very high cooling rates (around 50-70 °C/s) complete retention of the  $\beta$  phase, down to room temperature, was achieved. At intermediate cooling rates, a mixture of  $\alpha_2$  and  $\beta$  phase is observed with the  $\alpha_2$

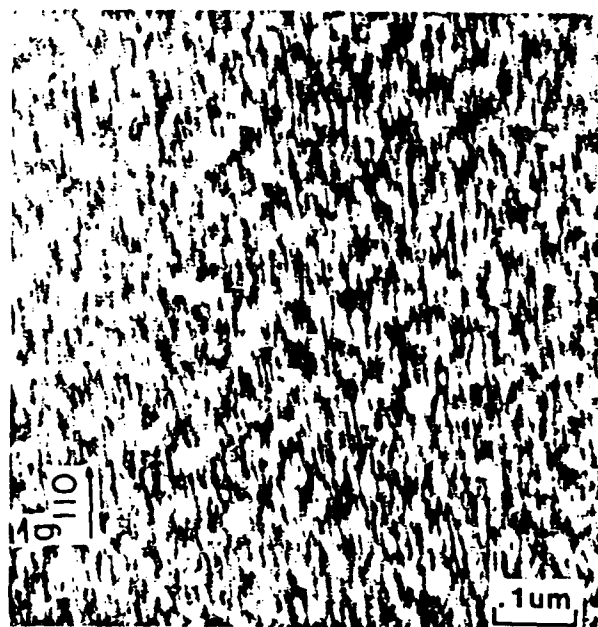
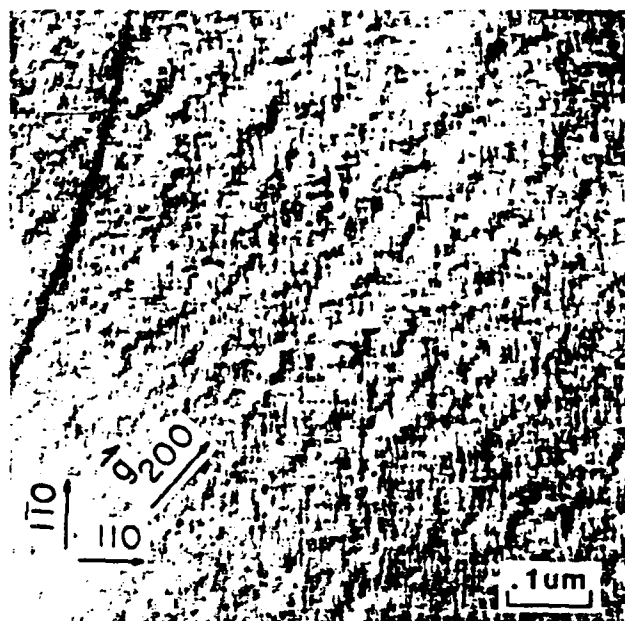
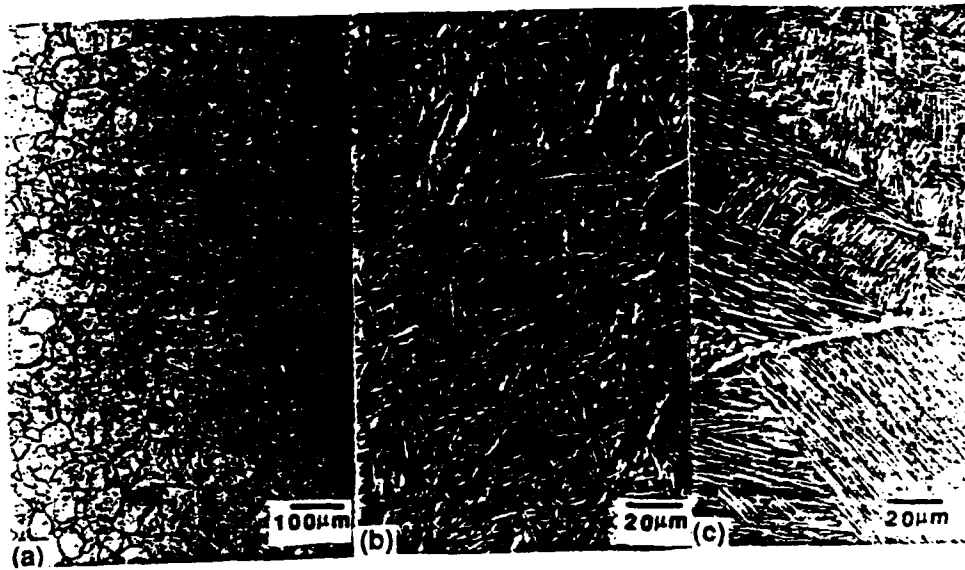


Figure 4. Mottled Microstructure of  $\omega$  Phase in  $Ti_3Al$  (Top) and Showing Streaking when Imaged in Two Beam Condition with  $g=\langle 110 \rangle \beta$  (Bottom)

getting coarser with decreasing cooling rates. Figure 5 shows the effect of cooling rates on the microstructure of a Ti-Al-Nb system [Ref. 15].



**Figure 5.** Effect of Cooling Rate in  $\text{Ti}_3\text{Al-Nb}$  from the  $\beta$  Region on Microstructure: (a)  $\beta$ /Air Cooling, (b)  $\beta$ /Controlled Cooling, (c)  $\beta$ /Slow Cooling

## **B. EFFECT OF ALLOYING ELEMENTS ON PHASE TRANSFORMATIONS AND MECHANICAL PROPERTIES**

### **1. Effect on Phase Transformations**

Alloying elements strongly influence both transformation temperatures and mechanical behavior of Ti-based alloys. It was shown [Ref. 16] in many binary alloys that the cooling rate at which there is a change in the mode of

transformation from nucleation and growth to shear, decreases with increasing alloying element addition. Studies on ternary element additions in the Ti-Al system, such as Nb [Ref. 17], have shown that alloys containing less than 5 at. pct. Nb transform martensitically to the hcp  $\alpha_2$  phase during quenching from the  $\beta$ -field. The subscript '2' indicates the ordering of  $\alpha$  phase into  $DO_{19}$  structure. In alloys with higher Nb content, the  $M_s$  temperature drops below room temperature. Figure 6 shows an equilibrium ternary section for the  $Ti_3Al+Nb$  system.

Recently, quaternary alloying additions have been made to the Ti-Al-Nb system with the view to further controlling transformations and to provide better mechanical properties and oxidation resistance. These alloys called 'super  $\alpha_2$ ' alloys have received a lot of attention with respect to their phase transformations [Ref. 14,15,20].

The effect of all these alloying additions on the phase transformations has not yet been evaluated and forms one of the objectives of this research that deals with a Ti-Al-Nb alloy with Ta and Cr additions for better oxidation resistance.

## **2. Effect on Mechanical Properties**

Alloy additions significantly affect the mechanical properties of Ti-based systems. Table I shows the effect of Al additions on the mechanical properties of Ti [Ref. 18]. It can be seen from the above table that increase of the aluminum content, causes improvement of the mechanical properties. Specifically, the

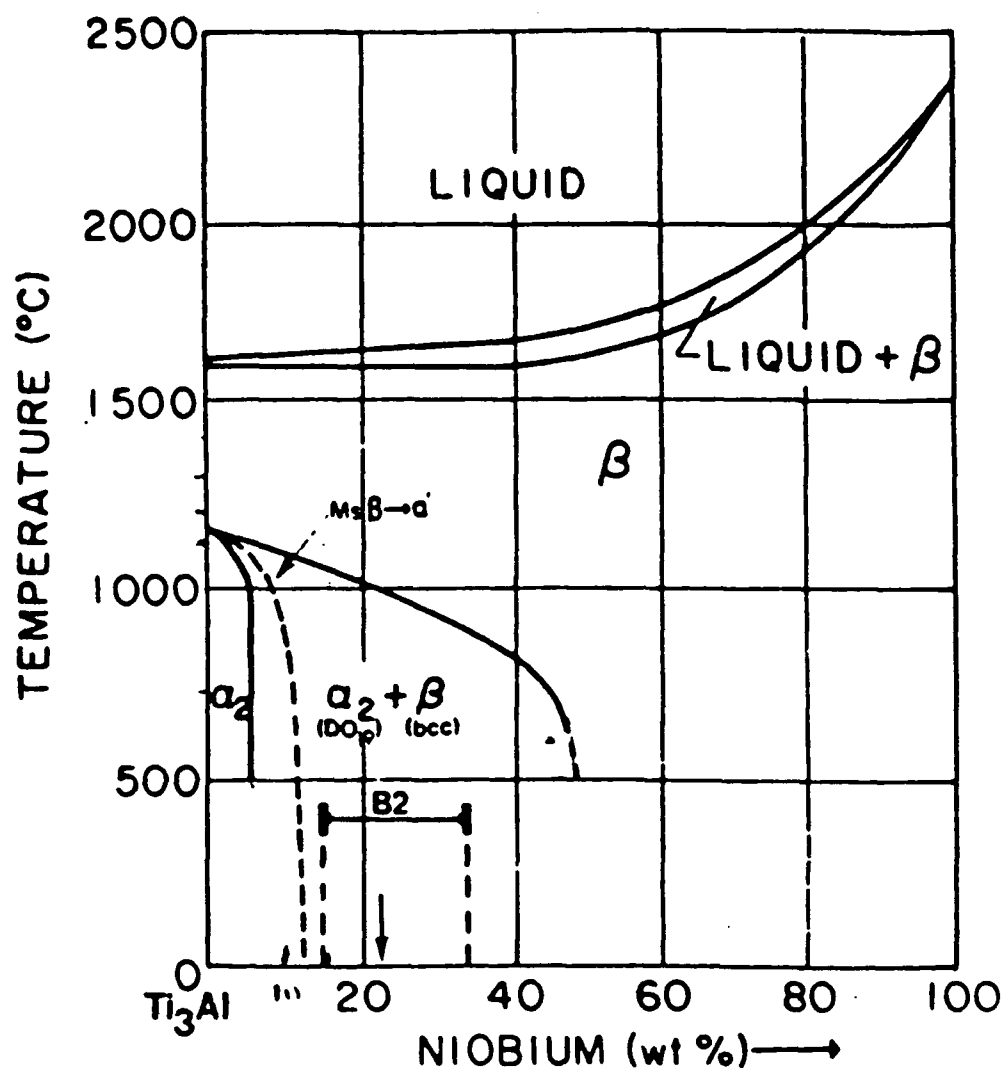


Figure 6.  $\text{Ti}_3\text{Al}$ +Nb ternary section [Ref. 17]

decrease in density and the increase in stiffness with increase in al content are the attractive properties of the Ti-Al system. The main disadvantage of the above system is its low ductility at room temperature. Lipsitt *et. al.*, [Ref. 19] found that in many of the Ti-Al systems, superdislocations are pinned by an unknown agent at room temperature. Thereby imparting significant brittle character to the microstructure. The pinning agent becomes ineffective at about 700 °C and allows dislocation mobility and hence an increase in ductility.

**TABLE I. PROPERTIES OF HIGH TEMPERATURE ALLOYS**

Property	Ti Base	Ti <sub>3</sub> Al	TiAl	Superalloys
Density (g/cm <sup>3</sup> )	4.5	4.1-4.7	3.76	8.3
Young's Modulus(GN/m <sup>2</sup> )	110-96	145-110	176	206
Max. Temp.- Creep(°C)	538	815	1038	1093
Max. Temp.-Oxidation(°C)	593	649	1038	1093
Ductility - R.T. (%)	20	2-5	1-2	3-5
Ductility-Operating(%)	High	5-8	7-12	10-20

Recently the effect of ternary and quaternary alloy additions on mechanical properties has attracted attention. Martin *et. al.*, [Ref. 20] on studying the effects of additions of Nb and W to TiAl and Ti<sub>3</sub>Al, found that these alloying elements increase the ductility and strength of the Ti-Al systems. A summary of their results is shown in Table II. The alloy compositions that they used are, Ti-27Al for  $\alpha_2$ , Ti-25Al-5Nb-1W for quaternary  $\alpha_2$ , Ti-50Al for  $\gamma$  and Ti-



49Al-2W for ternary  $\gamma$ , all atomic percentages. Their research resulted in the following conclusions:

1. The refinement of slip length in  $\text{Ti}_3\text{Al}$  base alloys causes a modest increase in ductility and a significant increase in strength.
2. Structural refinement in  $\text{TiAl}$  base alloys causes appreciable strengthening to occur without significantly decreasing the ductility. The high strength conditions also have significantly improved creep resistance.
3. Structural refinement can be accomplished through the control of the martensitic  $\beta \rightarrow \alpha$  phase transformation both by alloying and cooling rate control.
4. Additional slip length refinement can be attained through the secondary precipitation of  $\beta$ -phase stabilized by the presence of Nb and/or W.

### 3. Alloy Design

The chemical composition of the alloy under study is Ti-30 at.% Al-8 at.% Nb-2 at.% Cr-2 at.% Ta. The principle behind the alloy design was the retention of the high temperature ductile phase at room temperature and a stable mixture of  $\beta + \alpha_2$  at elevated temperatures. Niobium was found to be excellent  $\beta$  stabilizer since it increases nonbasal slip activity and retards ordering kinetics in  $\text{Ti}_3\text{Al}$  [Ref. 21]. Both Ta and Cr have also been reported to be  $\beta$  phase stabilizers [Ref. 22, 23]. Also all three alloy additions, Nb, Ta and Cr have been reported to increase oxidation resistance.

**TABLE II. AS EXTRUDED MECHANICAL PROPERTIES OF Ti-Al ALLOYS**

Alloy Designation	Temperature (°C)	0.2% Yield (MPa)	Ultimate (Mpa)	Plastic Elong.(%)	R.A. (%)
$\alpha_2$	25	-	552	-	0.1
Quaternary $\alpha_2$	25	796	920	0.4	1.1
$\alpha_2$	700	413	521	2.7	4.0
Quaternary $\alpha_2$	700	544	696	4.4	7.0
$\gamma$	25	335	450	0.9	1.6
Ternary $\gamma$	25	642	790	0.8	1.3
$\gamma$	700	300	360	14.0	22.0
Ternary $\gamma$	700	537	803	2.9	4.7

### C. X-RAY DIFFRACTION

X-ray diffractometry is a powerful tool in identifying the structure of crystalline materials. It is based on Bragg's law, which states that:

$$n\lambda = 2d\sin\theta \quad (1)$$

where  $\lambda$  is the wavelength of the incident x-radiation,  $d$  is the interplanar spacing of the crystal structure and  $\theta$  is the angle of reflection. The geometry of the x-ray diffraction is shown in Figure 7 [Ref. 24:p. 84]. The incident wave front XX' strikes the planes of atoms A,B,C and the diffracted energy is measured by the detector YY'.

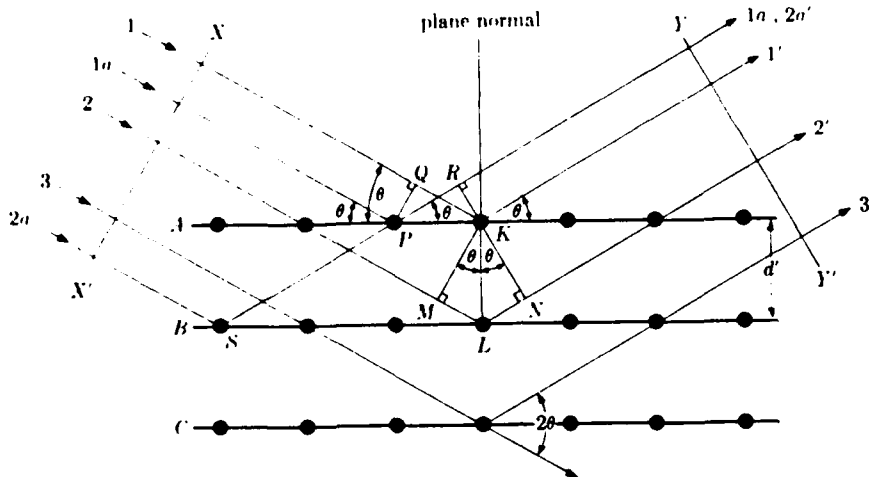


**Figure 7. Diffraction of X-Rays by a Crystal**

Lattice parameter calculations can be made by combining the Bragg's law and the planar spacing equation, which for the case of cubic systems is:

$$\frac{1}{d^2} = \frac{(h^2 + k^2 + l^2)}{a^2} \quad (2)$$

where  $a$  is the lattice parameter and  $h, k, l$  are the Miller indices. For a more accurate calculation of the lattice parameter a Nelson-Riley [Ref. 23 p.356] extrapolation will be used in this study.

#### **D. SCOPE OF PRESENT STUDY**

The scope of this research is to study the various phase transformations of the Ti-30 at.% Al-8 at.% Nb-2 at.% Ta-2 at.% Cr. The phase transformations of interest are  $\beta \rightarrow \alpha$ ,  $\beta \rightarrow \omega$ ,  $\alpha \rightarrow \alpha + \beta \rightarrow \beta$  and they were studied using scanning electron microscopy, transmission electron microscopy, dilatometry x-ray diffractometry and microhardness testing.

The specific goals of the research are:

1. to study the  $\beta_{\text{retained}} \rightarrow \alpha_2$  phase transformation in a  $\text{Ti}_3\text{Al}$  based alloy with additions of niobium, chromium and tantalum,
2. to study the effect of alloying element distribution on the microstructure and transformation kinetics,
3. to investigate the effect of alloying element on the ageing behavior of the retained  $\beta$  phase and the associated mechanical properties, and
4. to study the effect of cooling rate on the phase transformations in this alloy system.

## II. EXPERIMENTAL PROCEDURE

Two rods of Ti-30 at.% Al-8 at.% Nb-2 at.% Ta-2 at.%Cr alloy were obtained from Naval Air Research and Development Center. The samples were made via powder compaction and fabricated by Hot Isostatic Pressing in the  $\alpha+\beta$  region.

### A. HEAT TREATMENTS

Prior to heat treatment, thin disks were sliced off the rods and encapsulated in vycor glass tubes under  $10^{-5}$  Torr vacuum in order avoid oxidation due to high temperature. The glass tubes were sealed using a Hydrogen-Oxygen torch. The samples then heated at temperatures ranging from 1000°C to 1300°C for different times and ice-water quenched, breaking the glass tubes at the same time in order increase the cooling rates and retain the high temperature phases. The as quenched samples were then aged at temperatures between 500°C and 850°C and for times between 2 hours and 96 hours using an Argon atmosphere furnace. Some cooling rate variations were also performed from the high heat treatment temperatures. This was done in order to observe the effect of cooling rate on phase transformations.

## **B. MICROSCOPY**

### **1. Optical and Scanning Electron Microscopy**

Optical microscopy was conducted in order to analyze the microstructure of the as received, as quenched and the aged samples. Preparation of the mounted samples was made by first grinding on emery paper in successive steps from 240 to 600 grit and then polishing on diamond wheels using 6 and 1 microns diamond paste. Finally the samples were etched for 30 seconds in Kroll's reagent (5%HF, 20%HNO<sub>3</sub>, 75%H<sub>2</sub>O). The etched samples were examined in a Zeiss ICM 405 Photomicroscope at different magnifications and pictures were taken using Type 55 Polaroid film.

A Cambridge Stereo Scan S200 Scanning Electron Microscope and Kevex 8000 Energy Dispersive X-ray Analysis (EDX) Spectrometer were used for higher magnification observation and relative chemical composition of the various microconstituents.

### **2. Transmission Electron Microscopy**

Thin discs from the as received, as quenched and aged samples were cut using a low speed diamond saw. Three mm discs were machined out using a Metals Research Servomet Spark Machine Type SMD. The three mm discs were hand sanded to a thickness of 150 microns. The specimens were then electrochemically polished in a Struers Tenupol electropolishing device using a 6 percent perchloric acid, 59 percent methanol and 35 percent butyl alcohol

solution, cooled at -40 °C with liquid nitrogen. TEM experiments were carried out in a JEOL model 100 JEM CX transmission electron microscope operating at 120 KV.

### **C. DILATOMETRY**

An Orton Automatic Recording Dilatometer Model 15BC-1 was used in order to determine the transformation temperatures at various heating and cooling rates. Cylindrical samples one inch in length and 0.4 inches in diameter of the as quenched material were placed in the dilatometer under argon atmosphere. The relative expansion and contraction versus temperature of the samples for various heating and cooling rates were recorded using a X-Y plotter. The phase transformation temperatures were then determined by the changes in slope of the heating and cooling curves. A continuous cooling transformation diagram was generated using the results of the above experiment.

### **D. X-RAY DIFFRACTOMETRY**

Sample preparation for x-ray diffraction consisted of, first cutting thin discs out the material and then pulverizing them using a ceramic mortar and pestle. The powder was then mounted on the standard aluminum sample holder using amyl acetate.

A XRG-3100 Phillips X-Ray Generator controlled by a PW-1710 Phillips Diffractometer control unit was used for the x-ray diffraction. The generator was operated at 30 KV and 35 Ma. Data acquisition was done using a DEC 3100

Vaxstation. Peak intensities were recorded using a step scan of 0.05 degrees every two seconds was used. Samples of the as quenched and of the material aged at 500 °C, 650 °C and 750 °C for 2, 8 and 20 hours were analyzed by the above procedure in order to determine the crystal structures existing at each temperature after each aging time and calculate the lattice parameter of each.

#### **E. MECHANICAL TESTING**

There was an attempt made to do compression creep tests on the alloy using an Instron Universal Mechanical Testing machine model 6067 with a front clamp furnace attached to it. The machine was operated at constant load mode with a square wave load input. The attempt was unsuccessful because the grips that were used, made of a nickel superalloy, crept more than the tested samples.

Vickers microhardness measurements were taken on as quenched samples aged at 500 °C, 650 °C, 750 °C and 850 °C for 2, 6, 12, 24 and 48 hours. The readings were taken using a Buehler Micromet Microhardness Tester with a load of 200 grams. Samples were fine polished down to 0.5 microns before microhardness readings were taken. The results were plotted on a graph of Vickers microhardness vs aging time.



## IV. RESULTS

### A. MICROHARDNESS TESTING

The results of the Vickers microhardness measurements on the aged samples are shown in Figure 8. It can be seen that the samples aged at 650 °C exhibited the highest hardness, which remained almost constant after 24 hours of aging and was of the order of 600 on the Vickers hardness scale. Samples aged at 500 °C showed a similar behavior but approached slightly lower hardness values (~580). At higher temperatures microhardness decreased with increasing temperature and aging time. The rate of decrease was high up to 16 hours of aging at 750 °C and 850 °C, while for higher times it seemed to level off at around 520 (96h at 750 °C) and around 420 (96h at 850 °C). The error bars on the graph indicate the range of hardness values obtained for each heat treatment condition.

The above results suggest that there is a phase transformation occurring around 650 °C, which affects the mechanical behavior of the alloy. As it will be shown later, TEM of the sample aged at 650 °C for 96 hours showed the formation of a very fine acicular phase within the quenched in  $\beta$  phase matrix. The fact that the microhardness of all samples seemed to remain relatively constant after 24 hours of aging, indicates that the transformation kinetics for all the phase transformations exhibited by this alloy during aging are relatively fast.

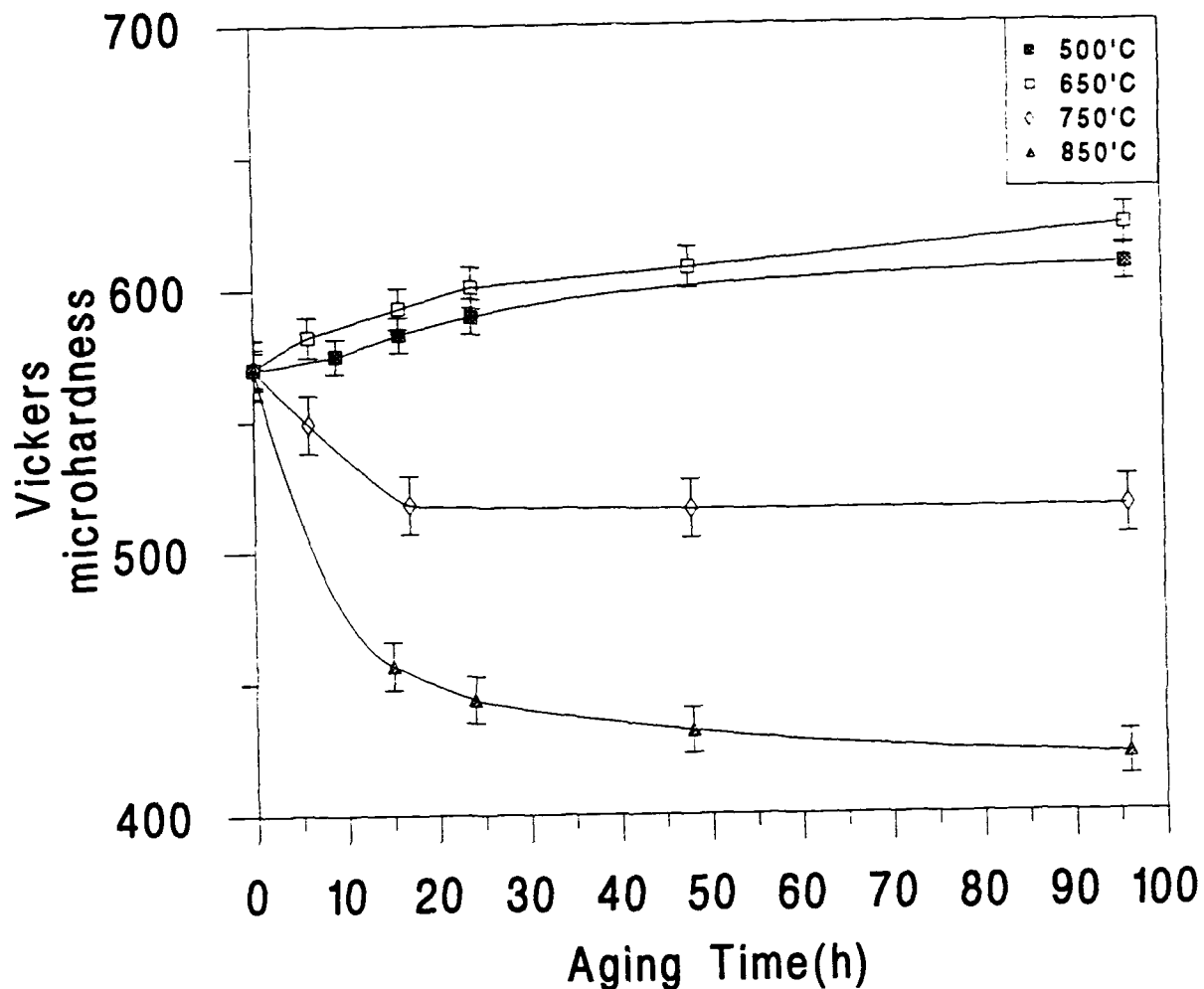


Figure 8. Vickers Microhardness of Quenched and Aged Samples vs Aging Time

On comparing the 750 °C and 850 °C curves, the lower hardness values obtained at the higher aging temperature indicate a microstructural change. From Figure 6 it is clear that at both temperatures, a two phase mixture of  $\beta$  (B2) and  $\alpha$  exists. Their relative amounts depend on the temperature. Hence a higher temperature should result in a larger proportion of  $\beta$ . Furthermore, a coarsening

effect might result in the same trends. This was confirmed by scanning electron microscopy (SEM) of the samples aged at 750 °C and 850 °C shown in Figure 9.

## B. X-RAY DIFFRACTION ANALYSIS

X-ray diffractometry was used in order to identify the phases present at each temperature after each aging time. Figure 10 shows the diffractometer output for the as quenched sample and for the samples aged at 500 °C for 4 and 24 hours. The primary phase identified in all three scans of Figure 10, using the JCPDS card files, was the B2. The extra peaks that are shown at  $2\theta$  angles of 38°, 44°, 65°, 78° and 82° are due to the aluminum sample holder that was used. Table III shows the peak positions and the associated relative intensities for the B2 phase in the as quenched sample.

**TABLE III. PEAK POSITIONS AND RELATIVE INTENSITIES**

Angle $2\theta$ (deg)	hkl	I/Imax (%)
39.3025	110	100
56.7525	200	12.42
71.4474	211	29.27
84.8500	220	7.10
97.8700	310	8.47
111.7775	222	6.47
126.9675	321	7.32

From the data shown in Table III and using the Nelson-Riley function which is:

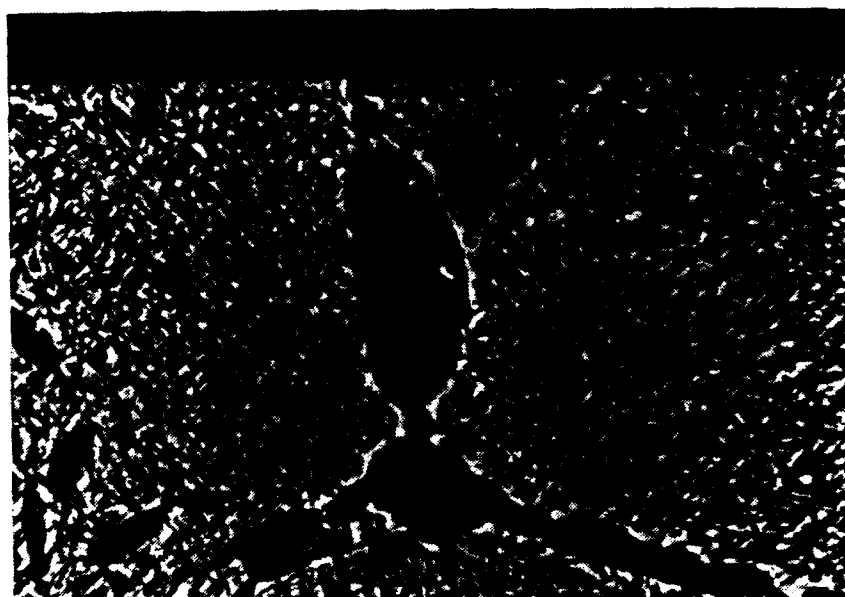
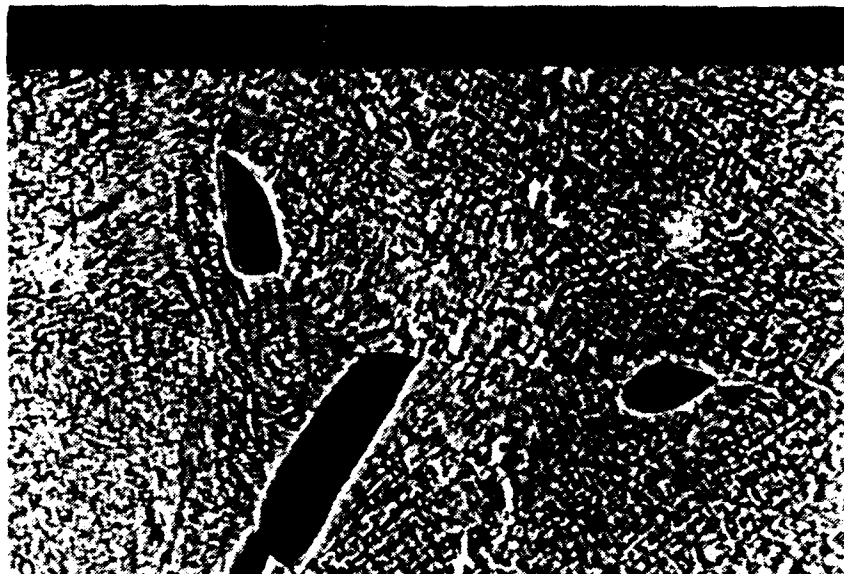


Figure 9. SEM Micrographs of the Samples Aged at 750°C (Top) and 850°C (Bottom) Showing Coarsening Effect Between the Two Temperatures

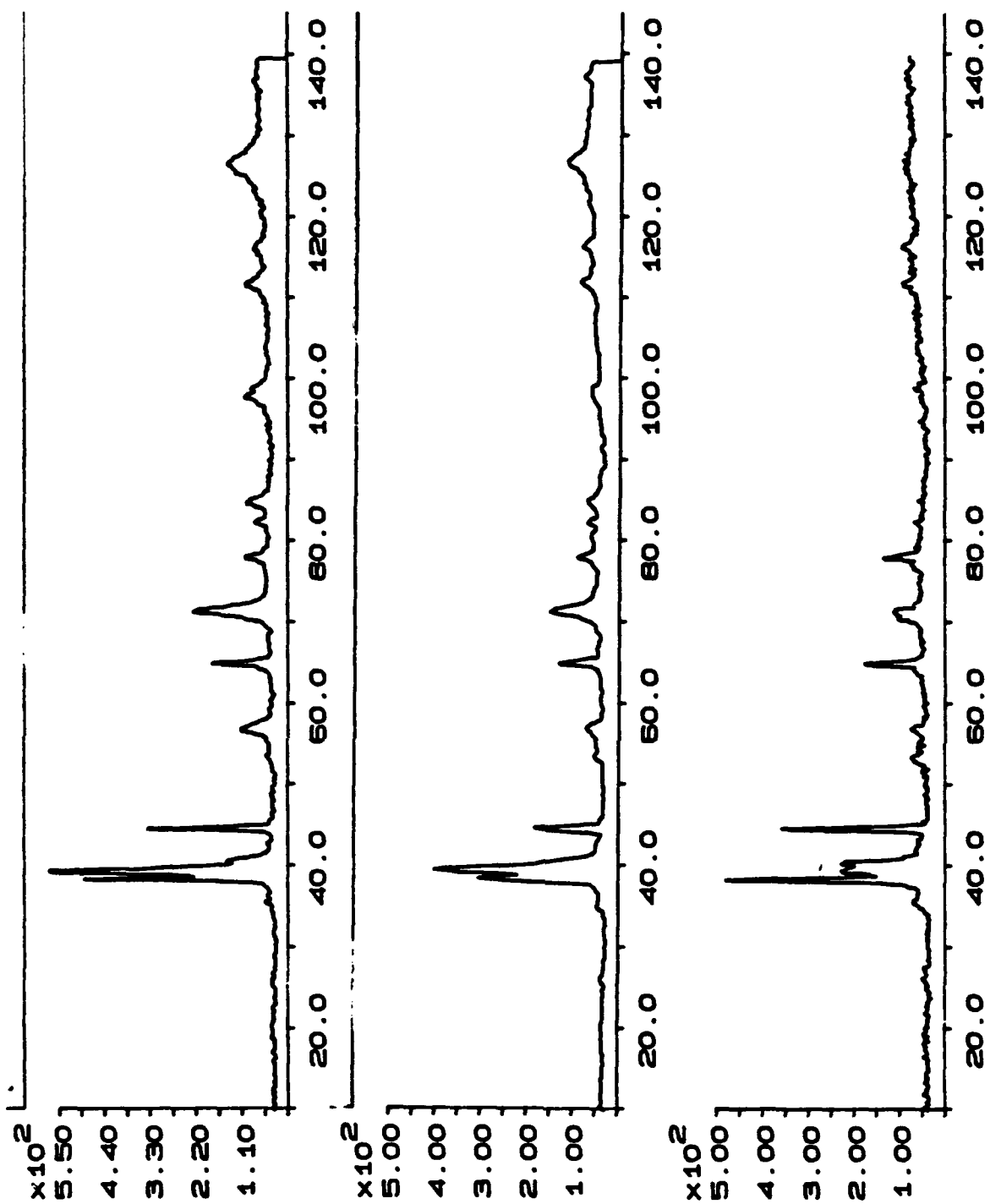


Figure 10. Diffractometer Output of Relative Intensities vs Angle  $2\theta$  for the As Quenched and the Samples Aged at 500°C for 4 and 24 Hours

From the data shown in Table III and using the Nelson-Riley function which is:

$$\left( \frac{\cos^2\theta}{\sin\theta} + \frac{\cos^2\theta}{\theta} \right) \quad (3)$$

the lattice parameter of the B2 structure was calculated by a Nelson-Riley extrapolation shown in Figure 11. A value of 3.22297 Å was obtained.

It can be seen from Figure 10 that aging at 500°C for 4h shows very small peaks at 35.6° and 53.2°. These correspond to the  $\alpha_2$  structure and seemed to be slightly intensified after 24h of aging. Hence the formation of  $\alpha_2$  is extremely sluggish at 500 °C and cannot be the reason of the increased hardness seen in Figure 8. Figures 12 and 13 show XRD scans for the samples aged at 650°C and 750°C for 2 and 24 hours respectively. The patterns in all four scans were matched to the JCPDS card number 9-98, which is the hexagonal close packed  $\alpha_2$  phase. Figure 13 shows that the  $\beta \rightarrow \alpha$  transformation has been completed after the first 2 hours of aging while at 650 °C (Fig. 12) the transformation is still incomplete after 24h.

The x-ray diffraction results show that the transformation of the quenched in  $\beta$  phase, to the equilibrium  $\alpha_2$  occurs very slowly below ~650 °C. At 500 °C, very small peaks from the  $\alpha_2$  can be seen to increase with aging time. Above this temperature the reaction accelerates and at 750 °C the XRD scans show a stable mixture of primarily  $\alpha_2$  and some retained  $\beta$ . Once again, the peaks from the Al sample holder can be used as an 'internal standard' to show that the relative

amounts of the  $\alpha_2$  and  $\beta$  phases change very little with aging time at this temperature.

It is believed that because of constraint effects the transformation of  $\beta \rightarrow \alpha$  is much more sluggish in the bulk sample used for the microhardness testing while the same transformation occurs more rapidly in the sample used for the X-ray analysis which was in powder form.

### C. MICROSCOPY OF HEAT TREATED SAMPLES

#### 1. 1200 °C and Quenched

Figure 14 shows a bright field (BF) TEM micrograph of the sample heat treated at 1200 °C for 2 hours and then ice-water quenched. High dislocation density can be seen in the matrix along with some lath-like features. Selected area diffraction pattern (SADP) from the matrix, shown in Figure 15, was indexed as the  $[001]\beta$  zone. The extra spots at  $\langle 100 \rangle$  show that this is the ordered b.c.c., called B2 (CsCl). Streaking in the  $\langle 110 \rangle$  is believed to be due to premartensitic effects [Ref. 13] and have been explained as being caused by lattice instabilities resulting in 'walls of intensity' in reciprocal space along  $g = \langle 110 \rangle$ . Very weak maxima are also seen at  $1/2 \langle 110 \rangle$ , i.e. positions where the streaks intersect.

Figure 16 is a BF micrograph showing mottled contrast in a lath-like feature and the surrounding matrix. Dislocation arrays form low angle grain boundaries between the lath and the matrix. The SADP from the matrix shown in Figure 17 is from the  $[113]\beta$  pole along with extra spots at  $1/2 \langle 112 \rangle$ . These

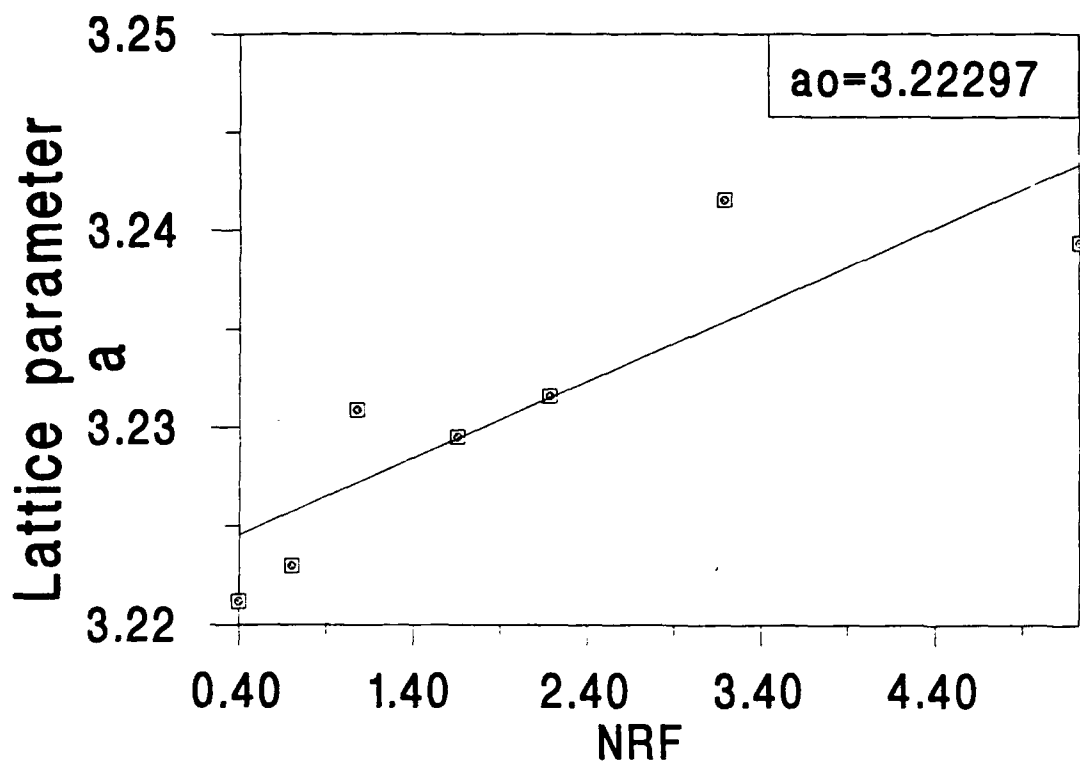


Figure 11. Nelson-Riley Extrapolation for Lattice Parameter 'a'



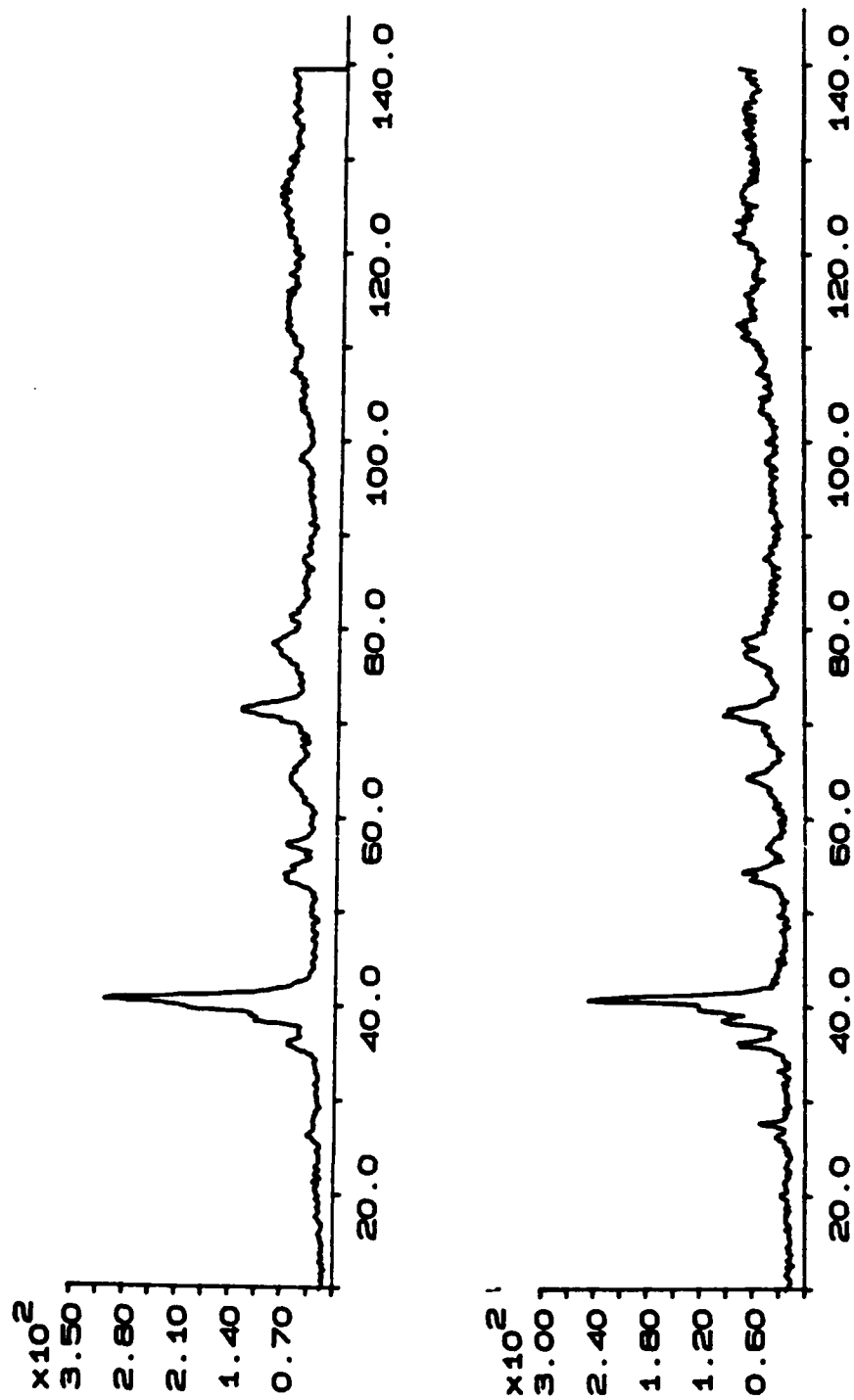


Figure 12. XRD Scans for the Sample Aged at 650°C for 2h (Top) and 24h (Bottom)

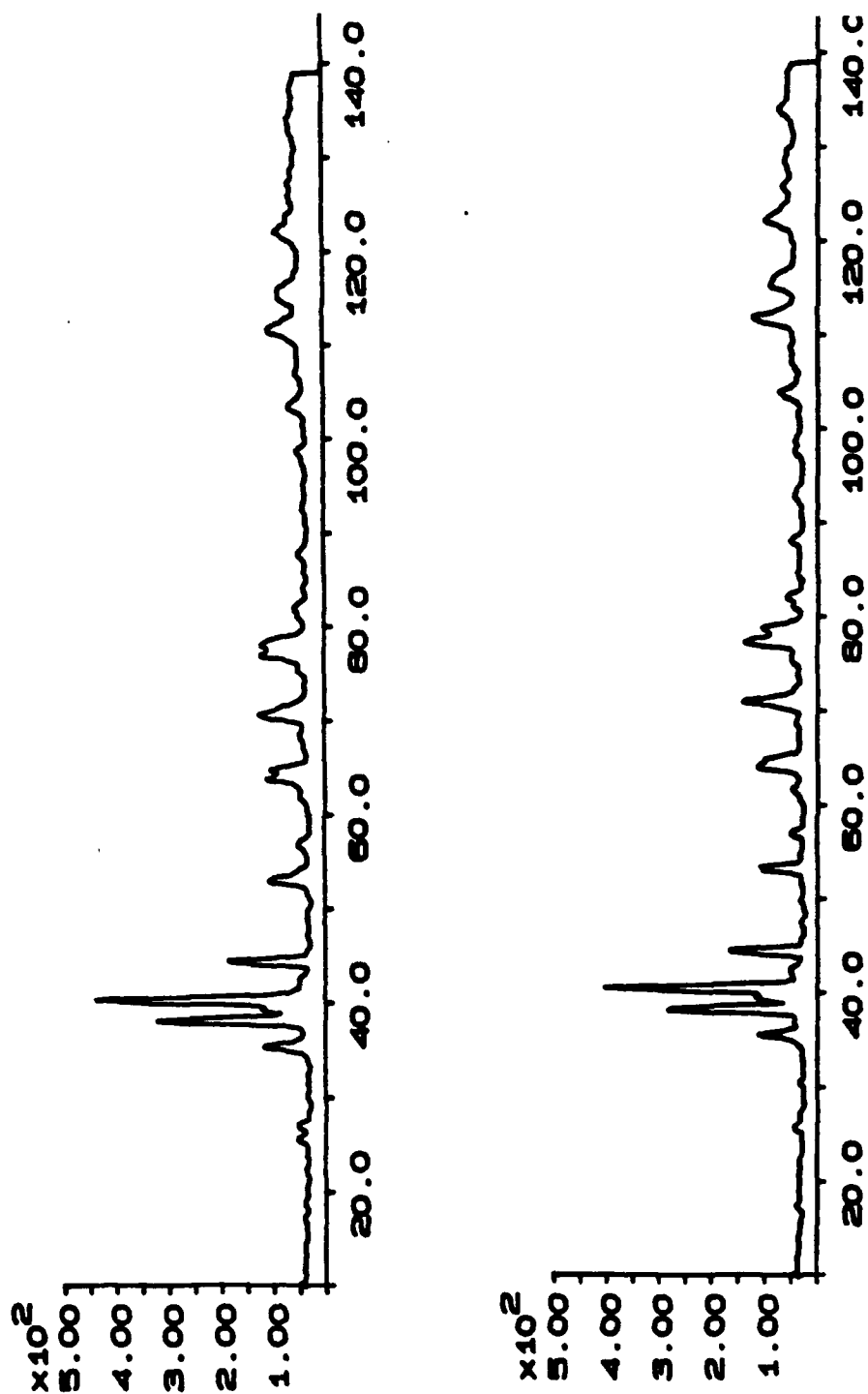


Figure 13. XRD Scans for the Sample Aged at 750°C for 2h (Top) and 24h (Bottom)

intensity maxima at  $1/2\langle 110 \rangle$  and  $1/2\langle 112 \rangle$  have been associated with the appearance of the tweed structure that is responsible for the mottled contrast seen in Figure 16. Streaking along the  $\langle 112 \rangle_\beta$  and  $\langle 110 \rangle_\beta$  type directions is observed. Extra spots at  $1/3\langle 112 \rangle_\beta$  type positions also appear and this is forbidden by structure factor considerations even after accounting for the formation of an ordered  $\omega$  phase. These diffuse maxima (at  $1/3\langle 112 \rangle$ ) are associated with an ordered ' $\omega$ -type' phase [Ref. 13] and appear to sharpen on aging, as will be shown later. Centered dark field with the  $1/2\langle 112 \rangle_\beta$  type spot did not show any features, but uniformly lit up both the lath and the matrix. This indicates the possibility that both the lath and the matrix might contain the same premartensitic phase. SADPs with both the matrix and part of a lath in the objective aperture showed only one type of diffraction pattern in the  $[001]_\beta$  orientation indicating that the matrix and the features are the same phase with a slight misorientation accommodated by the low angle grain boundary misfit dislocations.

Energy dispersive X-ray spectroscopy (EDXS) from regions inside the lath and the matrix are shown in Figure 18. It is evident that the matrix is rich in Ta and Cr and some form of segregation of these alloying elements occurs.

Another feature observed in the samples quenched from 1200 °C is the appearance of an orthorhombic phase. An SADP taken from one such region is shown in Figure 19 which is in the  $[001]_O$  orientation. This orthorhombic phase has been seen earlier [Ref. 5] in small regions near the  $\alpha_2$  lath structure. In this

alloy however, these regions appear as large grains that have a cuboidal shape, as observed by TEM.

Scanning electron microscopy on samples heat treated at 1300 °C for 4h and quenched, shown in Figure 20, showed similar segregation effects of Ta and Cr but only near the surface. Here the Ta and Cr poor regions had a cuboidal shape. At the center of the sample, only one phase was seen. The existence of a segregated region even after 4h at the elevated temperature of 1300 °C suggests that diffusional transport and depletion of Ta and Cr near the surface where protective oxide layers are formed, has to be responsible for the formation of



**Figure 14.** Bright Field from the Sample Heated at 1200 °C and Quenched, Showing High Dislocation Density Along with some Lath-Like Features



Figure 15. SADP [001]β Zone Showing Streaking Along <110>β and Superlattice Reflections at <100>

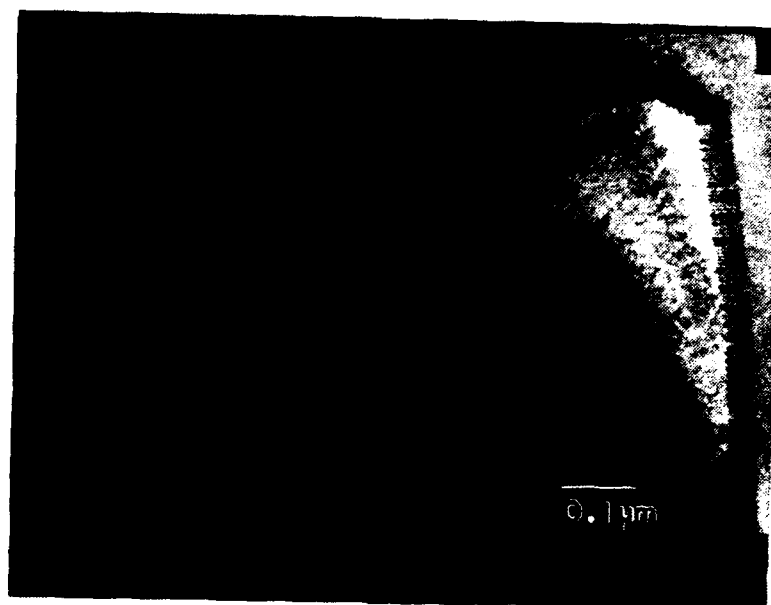
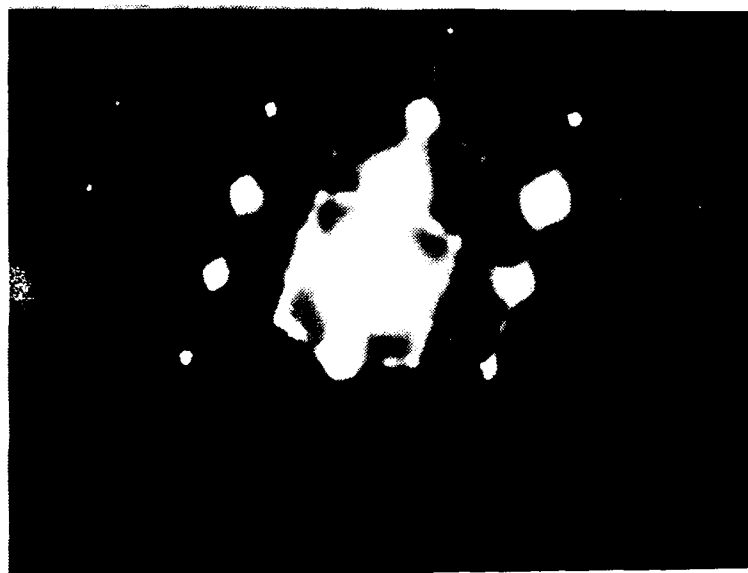


Figure 16. TEM micrograph from the As Quenched Sample Showing Mottled Contrast in Both the Lath and the Surrounding Matrix. Note Low Angle Grain Boundary Formed by Dislocation Array



**Figure 17. Selected Area Diffraction Pattern,  $[113]\beta$  Zone from the Matrix**

these cuboids. Generally, 1300 °C appeared to be high enough to result in only one single phase of  $\beta$ , as seen in Figure 20.

## **2. As Quenched and Aged at 500 °C for 9h**

Figure 21 shows a mottled contrast from the sample aged at 500 °C for 9 hours. A coarsening of the mottled structure can be seen compared to similar structures obtained in the as quenched sample. The selected area diffraction pattern from the same region shown in Figure 22 has been indexed as the  $[111]\beta$ . Intensity maxima at  $1/3\langle 110 \rangle$ ,  $2/3\langle 110 \rangle$  and streaking along  $\langle 110 \rangle$  are observed in this diffraction pattern. Also very distinct spots are seen at  $1/3\langle 112 \rangle$  and  $2/3\langle 112 \rangle$ . Related to the as quenched SADPs, these spots suggest the formation of the ordered ' $\omega$ -type phase' after 9h at 500 °C. Streaking along the  $\langle 110 \rangle$

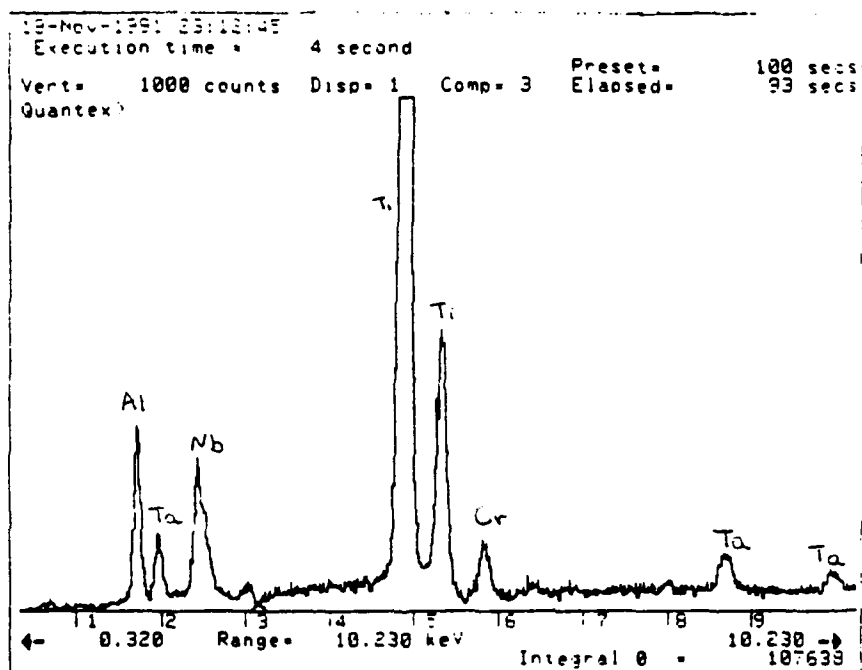
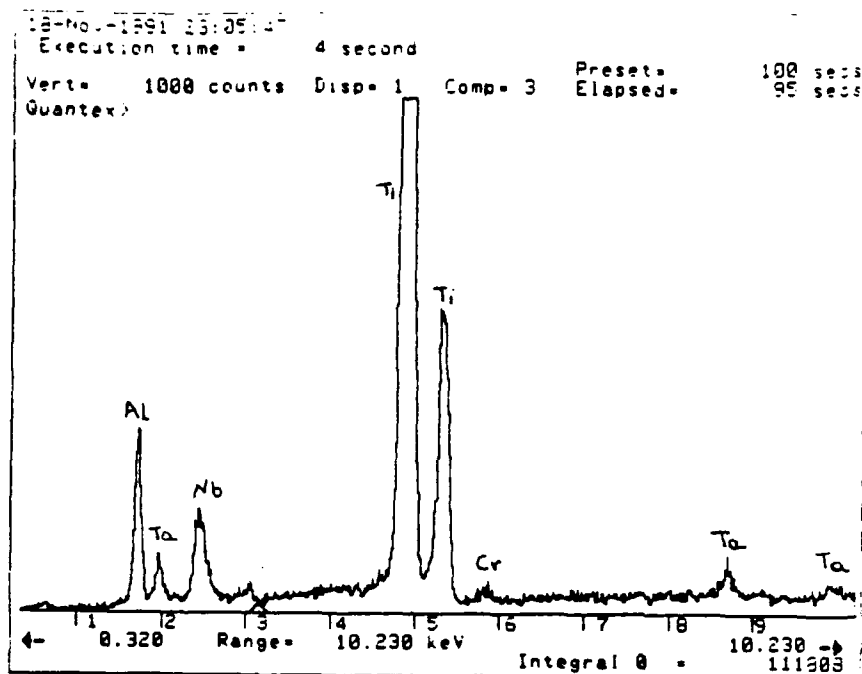
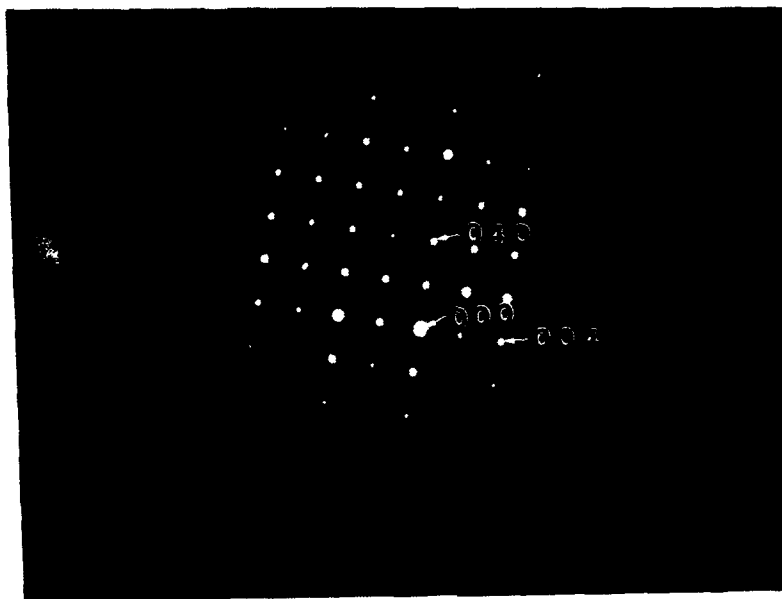


Figure 18. EDXS from Regions Inside (Top) and Outside (Bottom) a Lath, from the Sample Heated at 1200°C and Quenched



**Figure 19. Selected Area Diffraction Pattern [001]O Zone**

direction has been associated with 'premartensitic' effects in  $\beta$ -brass alloys and the intensity maxima at  $1/3$  and  $2/3\langle 110 \rangle$  can be explained by a premartensitic softening of the  $\{110\}\langle \bar{1}10 \rangle$  shear parameter  $1/2(C_{11}-C_{12})$  due to transverse lattice displacement wave vectors  $1/3\langle 110 \rangle$  and polarization vectors  $\langle \bar{1}10 \rangle$  [Ref. 25].

Figure 23 shows the  $[001]\beta$  SADP obtained from the same sample. The extra spots at  $\langle 100 \rangle$  are due to the B2 superlattice. Figure 24 is of the  $[113]\beta$  type zone showing similar effects. The above results show the condensation of diffuse maxima in the as quenched alloy into discrete spots, indicating the formation of



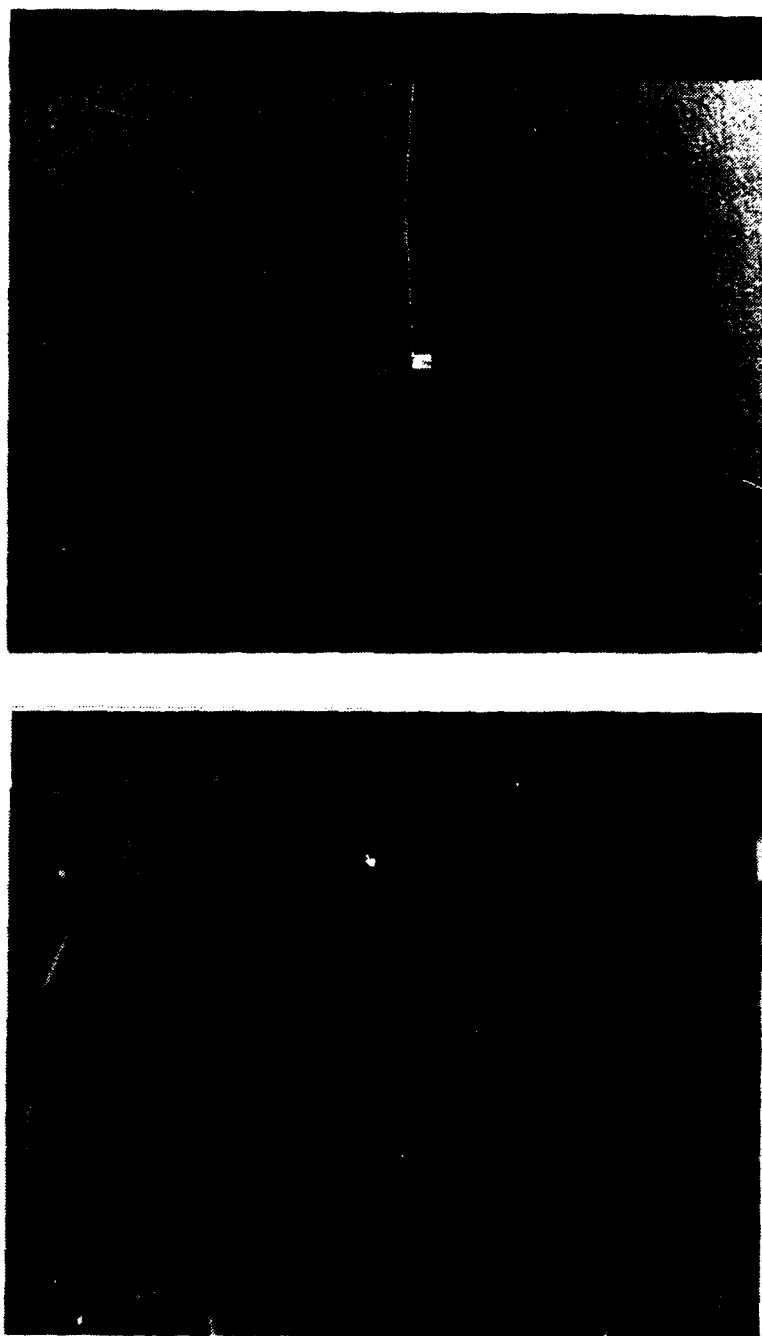
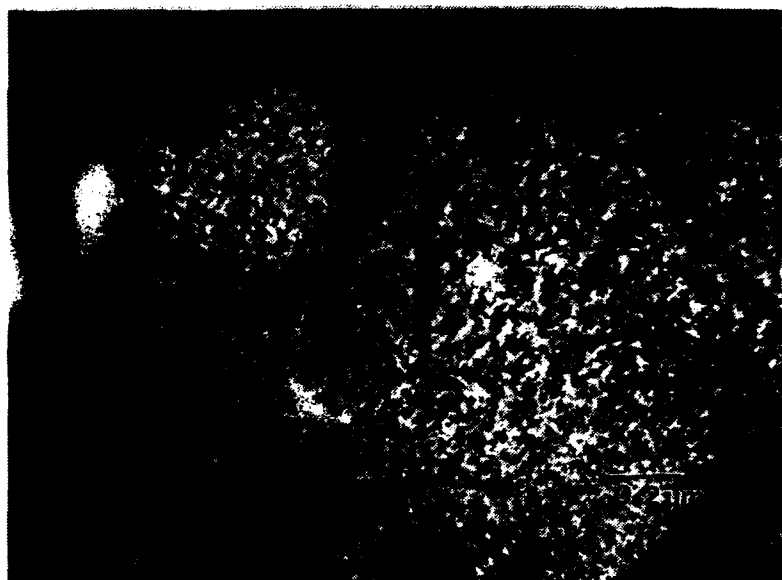


Figure 20. SEM Micrographs of the Sample Heated at 1300°C for 4h and Quenched, from Regions at the Center (Top) and Near the Surface (Bottom)



**Figure 21. Mottled Structure from the Sample Aged at 500°C for 9h**

the ' $\omega$ -type' phase while the premartensitic effects still exist after 9h at 500 °C. A similar ' $\omega$ -type' phase has been earlier shown to have the B8<sub>2</sub> structure [Ref. 13].

### **3. As Quenched and Aged at 650 °C for 48h**

Figure 25 shows a centered dark field TEM micrograph of the sample aged at 650 °C for 48 hours using the  $\langle 110 \rangle$  spot of the SADP shown in Figure

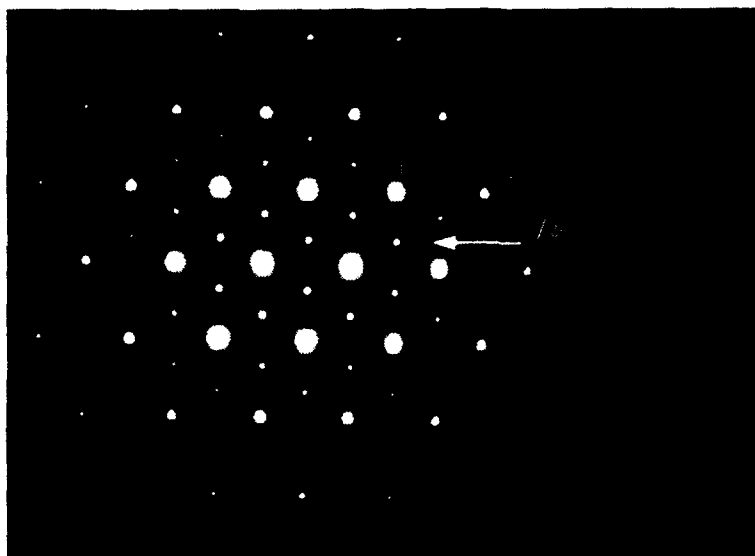


Figure 22. Selected Area Diffraction Pattern  $[111]\beta$  Zone

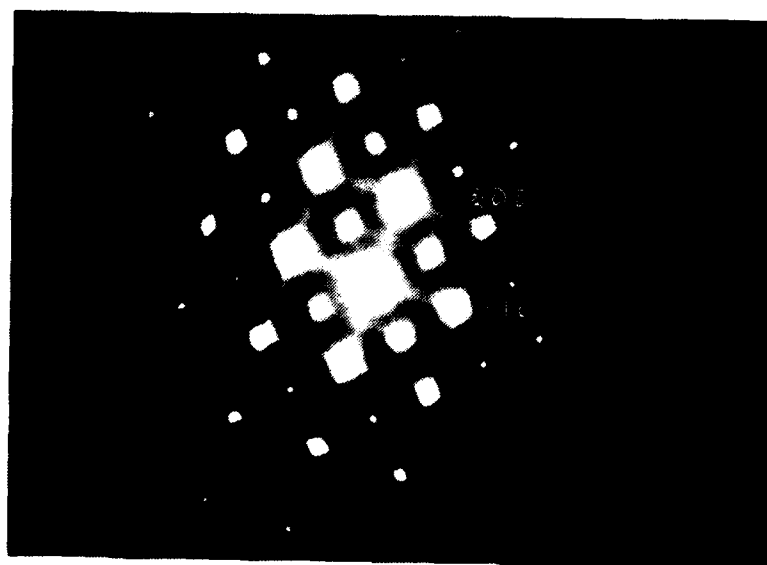
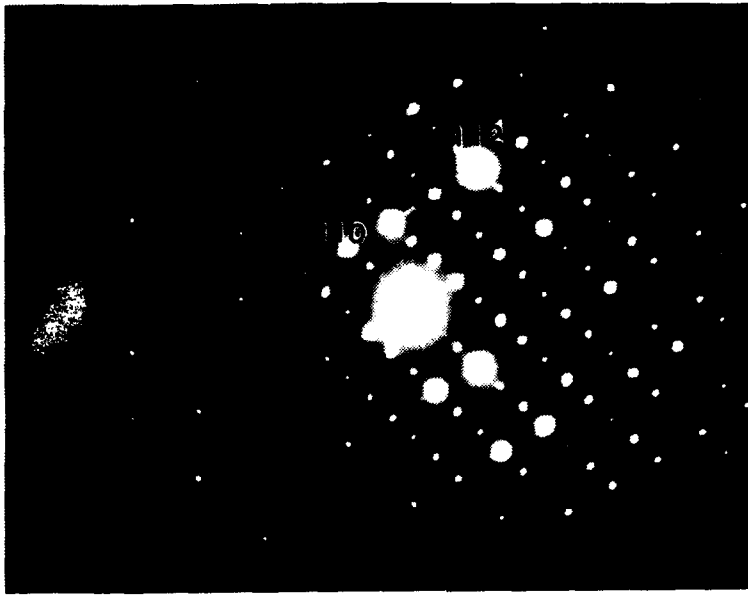


Figure 23. Selected Area Diffraction Pattern  $[001]\beta$  Zone



**Figure 24. Selected Area Diffraction Pattern [113]β Zone**

26. The light regions are the retained β phase imaged with the  $\langle 110 \rangle$  spot of the [113]β zone axis, while the fine needle-like structure is attributed to the beginning of the  $\alpha_2$  phase in keeping with the XRD results. Superimposed on the [113]β SADP in Figure 26, are a number of extra spots which are also attributed to the needle like phase in Figure 25.

#### **4. As Quenched and Aged at 850 °C for 48h**

Figure 27 shows a bright field micrograph of the sample aged at 850 °C for 48h. A two phase mixture consisting of laths of  $\alpha_2$  and regions of the β phase can be seen in this micrograph. Selected area diffraction from the β phase region can be seen in this micrograph. Selected area diffraction from the β phase region gave the [113]β zone pattern shown in Figure 28. Subsequent centered dark field (CDF) with the  $1/3\langle 112 \rangle$  type spot pointed to in the diffraction pattern resulted

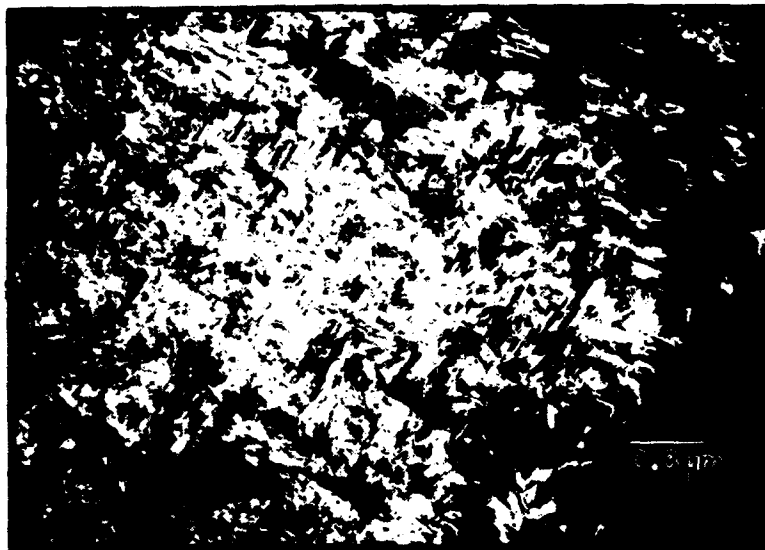


**Figure 25.** Dark Field TEM Micrograph of the Sample Aged at 650 °C Showing a Fine Needle-like Structure Due to the Formation of the  $\alpha_2$  Phase

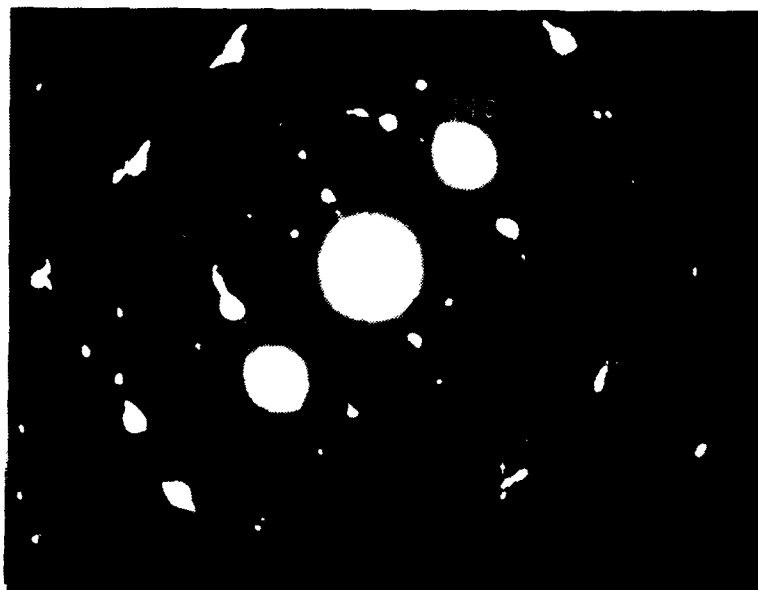


**Figure 26.** Selected Area Diffraction Pattern [113] $\beta$  Zone

in the micrograph of Figure 29. Recall that the  $1/3\langle 112 \rangle$  spots were attributed to the 'ω-type' phase. The laths that are lit up in Figure 29 are thus the 'ω-type' phase contained in the β phase, which appears in combination with the α<sub>2</sub> laths. Also, from the microhardness results, this combination appears to have the lowest hardness values.



**Figure 27.** Bright Field of the Sample Aged at 850°C for 48h Showing a Phase Mixture of α<sub>2</sub> Laths and β (with the ω-type phase)



**Figure 28.** Selected Area Diffraction Pattern  $[113]\beta$  zone, with  $1/3\langle 112 \rangle$  Spot Pointed and Used for CDF in Figure 29



**Figure 29.** Centered Dark Field of the Sample Aged at  $850^{\circ}\text{C}$  for 48h With the  $1/3\langle 112 \rangle\beta$  Type Spot Marked in Figure 28

#### D. DILATOMETRY

Dilatometry was used in this investigation in order to determine the phase transformation temperatures that are exhibited by this alloy and their dependence on the cooling rates. Initial microstructure during all experiments was that of the as quenched from 1200°C. Figure 30 shows typical dilatometer output for heating (at a rate of 2.5 °C/min, bottom curve) and cooling (at a rate of 1.8°C/min, top curve). It can be seen that the alloy exhibited two transformations during heating, i) centered ~650 °C and ii) centered ~920 °C. There is an indication of a third transformation starting at about 500 °C although the change in the strain vs temperature slope is extremely small. The transformation during cooling starts at ~1020 °C and ends at ~950 °C.

A possible explanation for the transformations that are seen in Figure 30 is that, during heating, between 650 °C and 710 °C the formation of the  $\alpha$  from the retained  $\beta$  occurs. This has been confirmed by TEM. From ~850 °C to ~1000 °C (i.e. centered about 920 °C) the transformation of  $\alpha \rightarrow \beta$  occurs for this heating rate. Above about 1000 °C the plot shows a straight line almost parallel to the initial section of the heating cycle and might be due to a similar phase i.e.  $\beta$ . This was earlier confirmed by TEM of samples quenched from 1100 °C which showed only retained  $\beta$  phase.

In the temperature range of 650 °C to 850 °C a phase mixture of  $\alpha + \beta$  exists. This agrees with the phase diagram shown in Figure 6. Transmission electron microscopy results of as quenched and aged at 850 °C samples, further supports



this conclusion. The transformation centered at  $-920\text{ }^{\circ}\text{C}$  represents the formation of  $\beta$  from the  $\alpha$  phase, which is completed at  $-1020\text{ }^{\circ}\text{C}$ .

On cooling, between  $1020\text{ }^{\circ}\text{C}$  and  $950\text{ }^{\circ}\text{C}$  the  $\alpha$  phase starts forming and below  $915\text{ }^{\circ}\text{C}$  a stable mixture of  $\alpha+\beta$  remains. The residual plastic strain remaining at room temperature might be explained due to microcracking and/or due to the difference in the phase composition before and after the completion of the thermal cycle, i.e. all  $\beta$  before heating and a mixture of  $\alpha+\beta$  after cooling.

According to the phase diagram shown in Figure 6 the relative amounts of  $\alpha$  and  $\beta$  should start changing continuously from temperatures above  $500\text{ }^{\circ}\text{C}$ . With increase in temperature (above  $650\text{ }^{\circ}\text{C}$ ) in the alloy studied, the transformation to  $\alpha$  occurs at the same time that lever law considerations applied to the two phase region, in Figure 6, indicate a competing mechanism for the transformation of  $\alpha\rightarrow\beta$ . This might explain the straight line portion of the heating curve between  $-700\text{ }^{\circ}\text{C}$  and  $900\text{ }^{\circ}\text{C}$ . Furthermore, on cooling, all the phase transformations are completed by  $-850\text{ }^{\circ}\text{C}$ . This cannot be explained by the phase diagram in Figure 6, even though the cooling rates used in Figure 30 are quit low ( $\sim 1.8\text{ }^{\circ}\text{C}/\text{min}$ ). Possible explanations for this are; i) a two phase region that shows no change in composition with temperature below  $850\text{ }^{\circ}\text{C}$ , or ii) the presence of  $\beta$  stabilizers like Ta and Cr.

Similar experiments with different cooling rates from  $1100\text{ }^{\circ}\text{C}$  yielded transformation temperatures that decreased with increasing cooling rates. In all cases the transformation of  $\beta\rightarrow\alpha$  was completed at temperatures below which a

stable two phase mixture existed. This resulted in the continuous cooling transformation diagram shown in Figure 31.

For cooling rates of 160 °C/min and above, the dilatometer output shown in Figure 32, showed only one drastic change in slope at 750 °C. Below that temperature the slope keeps changing at a very slow rate down to room temperature. A possible reason is that the  $\beta \rightarrow \alpha$  transformation starts at 750 °C but does not reach its stable  $\beta + \alpha$  mixture at room temperature. Further investigation needs to be done in order to verify the transformation occurring at that cooling rate and temperature.

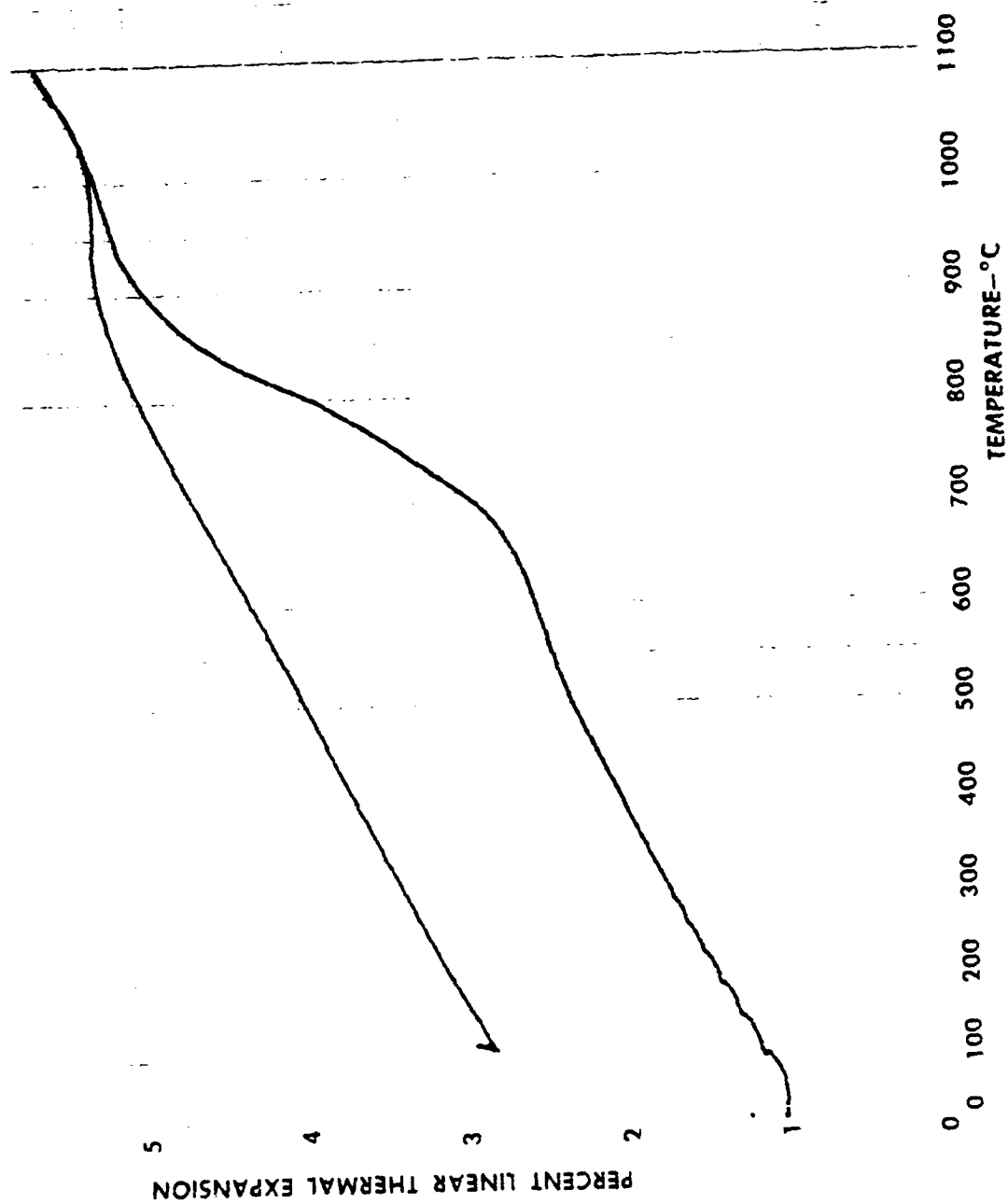


Figure 30. Dilatometry Curves of the As Quenched Sample. Heating (Bottom Curve) at a Rate of 2.5 °C/min and Cooling at a Rate of 1.8 °C/min

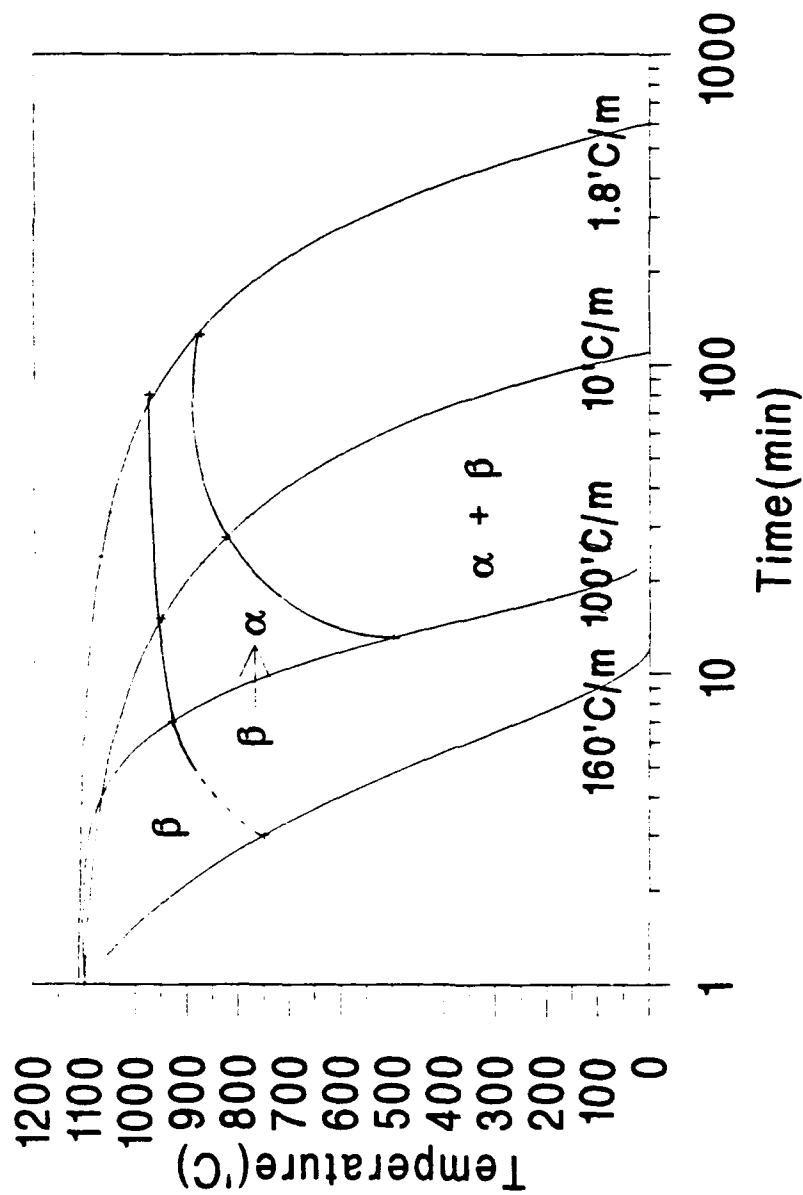


Figure 31. Continuous Cooling Transformation Diagram for the High Temperature  $\beta$  Phase

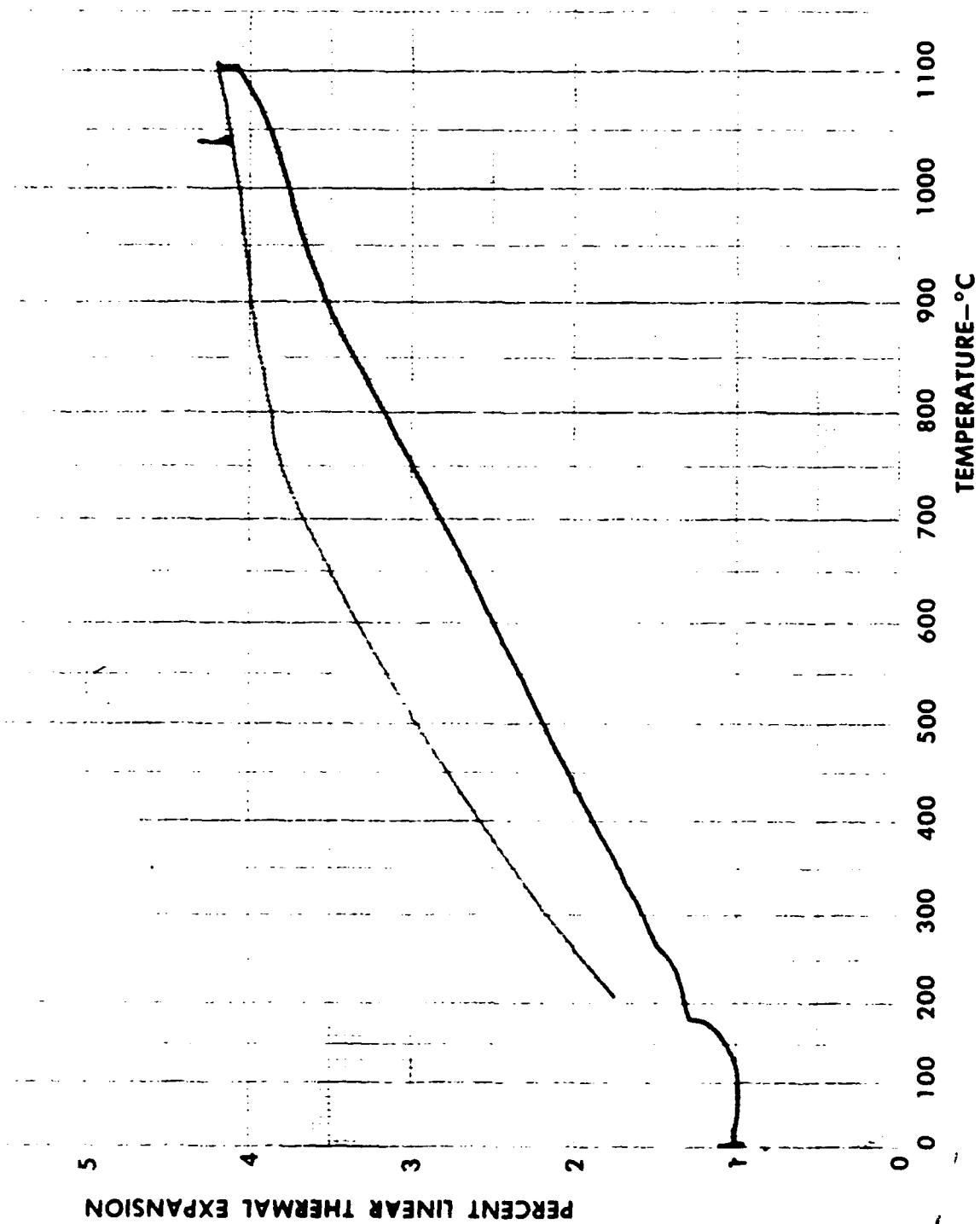


Figure 32. Dilatometry Curves of Slow Heating up to the  $\beta$  Region and Subsequent Cooling at a Rate of 160 °C/min

## V. CONCLUDING REMARKS

The present investigation dealt with the phase transformations that occur in a Ti-30 Al-8 Nb-2 Ta-2 Cr at.% along with their associated kinetics and mechanical properties, using scanning electron microscopy, transmission electron microscopy, x-ray diffraction analysis, microhardness testing and dilatometry.

On quenching this alloy from the high temperature  $\beta$  field (1200 °C), retention of the bcc phase occurs showing some lath-like features poor in Ta and Cr, and accommodated by misfit dislocations at low angle grain boundaries. This results in a 'pseudo two phase' mixture of  $\beta$ , one being richer in Ta and Cr than the other. Quenching from 1200 °C led to a cuboidal second phase that has tentatively been identified as an orthorhombic phase. The  $\beta_{\text{retained}}$  phase has the ordered B2 (CsCl) structure. It is believed that at the high temperature the  $\beta$  phase is not ordered, and that the ordering occurs during quenching. This is supported by the fact that no antiphase boundaries were observed in the as quenched sample. Upon aging  $\beta_{\text{retained}}$  at 500 °C, a second phase, the  $\omega$ , appears accompanied by streaking along  $\langle 110 \rangle$  and intensity maxima at  $1/3\langle 112 \rangle$  and  $\langle 110 \rangle$  in the selected area diffraction patterns. At 650 °C  $\beta$  phase starts transforming to  $\alpha_2$ , having a very fine acicular structure which exhibits peak hardness. Further aging at temperatures 750 °C and 850 °C coarsens the acicular structure resulting in a substantial drop of hardness. The microstructure at this

stage comprises a two phase mixture of  $\alpha_2$  and  $\beta$  (along with an ' $\omega$ -type' phase based on the B2).

Heat treating this alloy at temperatures of 1300 °C and above appears to result in a single retained phase indicating that the partitioning or segregation effects of the alloying elements are absent above 1300 °C. It is possible that this alloy goes through a two phase field ( $\beta$ +O) between temperatures of ~1100 °C to ~1300 °C, as the orthorhombic phase was also observed in samples quenched from 1100 °C and 1200 °C.

Dilatometry was used to construct a continuous cooling transformation diagram for the transformation of the high temperature  $\beta$  phase when cooled from 1100 °C. No distinction is made here between the transformations of the orthorhombic phase and the  $\beta$  phase and further work is required to identify the transformation behavior, if any, of the 'O' phase.

## LIST OF REFERENCES

1. Ogden, H.R., Maykuth, D.J., Finlay, W.L., and Jaffee, R.I., "Constitution of Titanium-Aluminum Alloys," *Transactions AIME*, Vol. 191, pp. 1150-1155, 1951.
2. Murray, J.L., in *Binary Alloy Phase Diagrams*, Vol. 1, pp. 225-227, ASM International, 1990.
3. Blackburn, M.J., in "The Science, Technology and Application of Titanium," *Proceedings of International Conference on Titanium*, pp. 633-643, London 21-24 May 1968.
4. JCPDS, "Powder Diffraction File - Inorganic Phases," International Center for Diffraction Data, Swarthmore, PA, 1987.
5. Banerjee D., Gogia, A.K., Nandy, T.K., and Joshi V., *Acta Metallurgica*, Vol. 36, pp. 871-882, 1988.
6. Konitzer D.G., Jones I.P., and Frazer H.L., *Scripta Metallurgica*, Vol. 20, p. 265, 1986.
7. Muraleedharan K., Nagender Naidu S.V., and Benarjee D., "Orthorhombic Distortions of the  $\alpha_2$  Phase in Ti<sub>3</sub>-Al-Nb Alloys: Artifacts and Facts," *Scripta Metallurgica et Materialia*, Vol. 24, pp. 27-32, 1990.
8. Collins, E.W., *Applied Superconductivity, Metallurgy and Physics of Ti Alloys*, Plenum Press, New York, 1986.
9. De Fontaine, D., "Mechanical Instabilities in the b.c.c. Lattice and the Beta to Omega Phase Transformation," *Acta Metallurgica*, Vol. 18, pp. 275-279, 1970.
10. Silcock, J.M., "An X-ray Examination of the Omega Phase in TiV, TiMo, and TiCr Alloys," *Acta Metallurgica*, Vol. 6, pp. 481-493, 1958.
11. Sass, S.L., "The Structure and Decomposition of Zr and Ti b.c.c. Solid Solutions," *J. Less-Common Metals*, Vol. 28, pp. 157-173, 1972.
12. Perkins, J., Delaey, L., and Massalski, T.B., *J. Material Science*, Vol 7, p. 1197, 1972.



13. Strychor, R., Williams, J.C., and Soffa, W.A., "Phase Transformations and Modulated Microstructures in Ti-Al-Nb Alloys," *Metallurgical Transactions*, Vol. 19A, pp. 225-234, 1988.
14. Baeslack, W.A. III, and Broderick, T., "Effect of Cooling Rate on the Structure and Hardness of a Titanium Aluminide," *Scripta Metallurgica et Materialia*, Vol. 24, pp. 319-324, 1990.
15. Cho W., Thompson A.W., and Williams, J.C., "Creep Behavior of Ti-25Al-10Nb-3V-1Mo," *Metallurgical Transactions*, Vol. 21A, pp. 641-651, 1990.
16. Jepson, K.C., Brown, A.R.G., and Gray, J.A., in "The Science Technology and Application of Titanium," *Proceedings of an International Conference of Titanium*, pp. 677-690, London, 21-24 May 1968.
17. Nartova, T.T., and Sopochkin, G.G., *Russian Metallurgy (Metally)*, Vol. 2, p.138, 1970.
18. Lipsitt, H.A., "Titanium Aluminides-An Overview," *Proceedings of the Materials Research Society Symposium*, Vol. 39, pp. 351-364, 1985.
19. Lipsitt, H.A., Shechtman, D., and Schafrik, R.E., "The Deformation and Fracture of  $Ti_3Al$  at Elevated Temperatures," *Metallurgical Transactions*, Vol. 11A, pp. 1369-1375, 1980.
20. Martin, P.A., Lipsitt, H.A., Numfer, N.T., and Williams, J.C., "The Effects of Alloying on the Microstructure and Properties of  $Ti_3Al$  and  $TiAl$ ," *Proceedings of the 4th International Conference on Titanium*, Japan, pp. 1245-1254, November 1980.
21. Sastry, S.M.L., and Lipsitt, H.A., in "Ti'80 Science and Technology," edited by H. Kimura and O. Izumi, *TMS-AIME*, pp. 1231-1243, Warrendale, PA, 1980.
22. Maykuth, D.J., Ogden, H.R., and Jaffe, R.I., "Titanium-Tungsten and Titanium-Tantalum systems," *Transactions AIME*, Vol. 197, pp. 231-237, 1953.
23. Spachner, S.A., "Comparison of Structure of Omega Transition Phase in Three Titanium Alloys," *Transactions AIME*, Vol. 212, p. 57, 1958.
24. Cullity, B.D., *Elements of X-Ray Diffraction*, Second Edition, Addison-Wesley, 1978.

25. Sandroock, G.D., Perkins, A.J., and Hehemann, R.F., "The Premartensitic Instability in Near-Equiatomic TiNi," *Metallurgical Transactions*, Vol. 2, pp. 2769-2781, 1971.

## INITIAL DISTRIBUTION LIST

		No. of Copies
1.	Defense Technical Information Center Cameron Station Alexandria, VA 22304-6145	2
2.	Library, Code 52 Naval Postgraduate School Monterey, CA 93943-5002	2
3.	Naval Engineering Curricular Office Code 34 Naval Postgraduate School Monterey, CA 93943-5000	1
4.	S. Mitra, Code ME/Mt Department of Mechanical Engineering Naval Postgraduate School Monterey, CA 93943-5000	1
5.	A.J. Healey, Code ME/Hy Department of Mechanical Engineering Naval Postgraduate School Monterey, CA 93940-5000	1
6.	Naval Attache Embassy of Greece 2228 Massachusetts Ave., NW Washington, D.C. 20008	3
7.	E. Tsourdalakis Zakinthou 8 A. Ilioupolis 16343 Athens, Greece	2